Complex interplay of forcings drives Indian vegetation and summer monsoon variability during MIS 11

Dulce Oliveira[1,2], Stéphanie Desprat[3,4], Qiuzhen Yin[5], Coralie Zorzi[1,2], Zhipeng Wu[5], Krishnamurthy Anupama[6], Srinivasan Prasad[6], Montserrat Alonso-García[7], Philippe Martinez[3]

[1] Centre of Marine Sciences (CCMAR/CIMAR LA), Universidade do Algarve, 8005-139 Faro, Portugal
[2] Divisão de Geologia e Georecursos Marinhos, Instituto Português do Mar e da Atmosfera (IPMA), 1495-165 Algés, Portugal
[3] Université de Bordeaux, CNRS, Bordeaux INP, UMR 5805 EPOC, F-33600 Pessac, France
[4] Ecole Pratique des Hautes Etudes (EPHE), PSL University, Paris, France
[5] Earth and Climate Research Center, Earth and Life Institute, Université Catholique de Louvain, Louvain-la-Neuve, Belgium
[6] French Institute of Pondicherry (IFP), Laboratory of Palynology & Paleoecology, CNRS-MAEE, Pondicherry 605001, India
[7] Faculty of Sciences, Department of Geology (Paleontology), Universidad de Salamanca, 37008 Salamanca, Spain

Correspondence to: Dulce Oliveira (dulce_oliveiraa@hotmail.com)

Abstract. Marine Isotope Stage (MIS) 11 has long been considered a unique Quaternary interglacial stage due to its orbital similarities with the Holocene, persistent high atmospheric CO_2 concentrations and its extended duration, which triggered an unusual polar ice-sheet loss. Despite its importance, variability of the Asian summer monsoon, as well as its impacts on vulnerable tropical forests, during MIS 11 remain unexplored. Here, we document, for the first time, the vegetation and monsoon changes in eastern peninsular India and their underlying forcings using pollen analysis from IODP Site U1446, strategically retrieved from the Bay of Bengal to record changes in the summer monsoon rainfall in the core monsoon zone of India. Our results reveal the distinct roles of insolation, CO_2, ice volume, and millennial-scale variability in driving vegetation and summer monsoon changes, depending on the changing boundary conditions throughout MIS 11. Site U1446 pollen data, supported by model simulations, indicate that the maximum tropical forest expansion and strongest monsoon activity during the interglacial period (MIS 11c) followed boreal summer insolation, revealing the dominant role of insolation under a warm climate state with high CO_2 and reduced ice volume. Conversely, during the late MIS 11 (MIS 11b-a), the tropical forest decreased despite high insolation, indicating that expanding ice sheets and lower CO_2 overshadowed the insolation influence on the summer monsoon. Millennial-scale variability during late MIS 11 likely played an additional role in counteracting the response of the summer monsoon to insolation. Abrupt forest contractions, tied to low monsoon rainfall and southward shifts of the intertropical convergence zone, are attributed to ice sheet dynamics and ocean circulation disturbances. These events were rapidly followed by pronounced forest expansions, linked to northward shifts of the intertropical convergence zone, reinvigorations of deep ocean circulation, and CH_4 overshoots. Conspicuously, the first and most severe forest setback interrupted the full interglacial conditions of MIS 11, suggesting that extreme summer monsoon weakening could also occur under similarly warm future conditions. Our findings provide new insights into monsoon behavior during MIS 11, highlighting its high sensitivity to climate changes in the context of projected summer monsoon intensification and its effect on the tropical forest, which is a key component of both global carbon and methane cycles.

1. Introduction

The Indian Summer Monsoon (ISM) stands as the dominant subsystem of the Asian summer monsoon in terms of energy exchange, representing one of the strongest expressions of Earth's atmospheric-oceanic hydroclimate interactions. It accounts for up to 80-90% of Central India's annual rainfall in the so-called Core Monsoon Zone (CMZ), where it has its most representative expression and impacts millions of people and countless ecosystems (Gadgil, 2003). ISM-driven droughts, floods, landslides and other extreme events are among the most destructive natural hazards, causing widespread loss of life, severe socioeconomic disruption and irreversible ecosystems changes (e.g., IPCC 2022). With projections of an intensified global water cycle, including more frequent and severe extreme events, and persistent model uncertainty, predicting ISM variability remains a scientific priority (Turner and Slingo, 2009; Katzenberger et al., 2022). Inevitably, this leads to the study of ISM dynamics over geological times to assess its natural variability and the responses of vulnerable ecosystems, such as tropical forests, under globally warm interglacial conditions comparable to the present and near future.

Paleoclimate records of the two main Asian monsoon subsystems - the ISM and East Asian summer monsoon– encompassing several or all key interglacials of the last 800 ka (Past Interglacials Working Group of PAGES, 2016) have relied on (1) Indian and Chinese speleothems, loess deposits and lake sediments (e.g., Zhisheng et al., 2011; Cheng et al., 2016; Kathayat et al., 2016; Sun et al., 2019; Zhang et al., 2019; Zhao et al., 2020; Gao et al., 2024), (2) marine sequences from the Arabian Sea, South China Sea and Bay of Bengal (e.g., Clemens and Prell, 2003; Ziegler et al., 2010; Caley et al., 2011; Bolton et al., 2013; Clemens et al., 2018, 2021; Gebregiorgis et al., 2018; Alonso-Garcia et al., 2019; Bhadra and Saraswat., 2022), and (3) model simulations, including data-model comparisons (Kutzbach, 1981; Kutzbach et al., 2008; Lyu et al., 2021; Sun et al., 2019; Sun et al., 2022). Since Kutzbach's (1981) seminal work on the Holocene, northern hemisphere summer insolation has been widely recognized as the dominant driver of the orbital-scale variability of the Asian summer monsoon, principally due to its influence on land-ocean thermal gradients. Nonetheless, conflicting trends between these monsoon records have generated extensive debate over the past three decades about the role of insolation versus internal forcings (see Cheng et al., 2022 for a recent review). Contrary to the "zero phase" view of a predominant precession rhythm and near-zero phase lag (e.g., Kutzbach et al., 2008; Cheng et al., 2016; Zhang et al., 2019; Bhadra and Saraswat., 2022), several studies have found dominant obliquity and eccentricity cycles, or combined 100, 41, and 23-kyr periodicities, and a precession phase lag of ~5-10 ka (e.g., Clemens and Prell, 2003; Ziegler et al., 2010; Caley et al., 2011; Bolton et al., 2013; Gebregiorgis et al., 2018; Clemens et al., 2021; Gao et al., 2024). These findings suggest a stronger influence of internal feedback mechanisms, related to global ice volume and atmospheric CO_2 concentrations, which may be linked to the transport of moisture from the Southern Hemisphere (e.g., Clemens et al., 2021). Beyond the complexity of deciphering these paradoxical results by evaluating which proxy and model reconstructions most accurately capture the monsoon dynamics, recent studies from the CMZ of India have reinforced the need to differentiate the ISM and the East Asian summer monsoon subsystems mostly due to their distinct sensitivities to forcing mechanisms and moisture sources (Pan et al., 2017; Nilsson-Kerr et al., 2019; 2021). Yet, compared to the East Asian summer monsoon, the ISM monsoon rainfall is considerably less documented, especially within India's CMZ where evidence from interglacials older than the Holocene is restricted to the long marine sequence of the Integrated Ocean Drilling Program (IODP) Site U1446, located on northeast Indian margin. Records from this site, based on leaf wax isotopes, sea surface temperatures (SST), planktonic and benthic seawater $\delta^{18}O$, X-ray fluorescence (McGrath et al., 2021; Clemens et al., 2021), and planktic foraminifera assemblages (Bhadra and Saraswat, 2022), primarily focus on orbital-scale ISM variations across late Pleistocene glacial-interglacial cycles, which precludes a precise characterization of the ISM's response solely to interglacial boundary conditions. To date, past interglacial ISM variability in the CMZ has only been explored through comparisons between the Holocene (12–0 ka) and MIS 5e (130-116 ka). Vegetation and salinity reconstructions from Site U1446 indicate stronger ISM activity during MIS 5e due to higher insolation (Clément et al., 2024). In contrast, regional data-model comparisons show that the Asian summer monsoon was the only boreal system to show a reduced monsoon activity during MIS 5e compared to the Holocene (Nilsson-Kerr et al., 2021), in line with multiproxy data from the northern Bay of Bengal (Wang et al., 2022). These inconsistencies highlight the complexity of proxy sensitivity and the heterogeneous responses of monsoonal subsystems to various forcings, underscoring the need for more targeted proxy reconstructions and data-model comparisons within India's CMZ during past warm intervals.

Here we focus on MIS 11 (426-374 ka), a period extensively studied mainly owing to the potential astronomical analogy of its interglacial substage MIS 11c (426-396 ka) with the Holocene (Berger and Loutre, 2002; Droxler et al., 2003; Candy et al. 2014; Past Interglacials Working Group of PAGES, 2016; Tzedakis et al., 2022). Moreover, it presents a unique combination of relevant characteristics for ongoing and projected climate change, including prolonged CO_2-driven climate warming, higher-than-present sea level linked to the loss of Greenland and West Antarctic ice sheets, remarkable Arctic warmth, sustained North Atlantic warming, an Atlantic meridional overturning circulation (AMOC) comparable or stronger-than-present, and persistent abrupt climate change throughout MIS 11 (e.g., Lisiecki and Raymo, 2005; Jouzel et al., 2007; Melles et al., 2012; Candy et al., 2014; Grant et al., 2014; Dutton et al., 2015; Yin and Berger, 2015; Snyder, 2016; Hu et al., 2024). The majority of MIS 11 research has targeted the mid- to high-latitudes of the northern hemisphere, with a notable focus on the response of European vegetation (Candy et al., 2014; 2024). In contrast, studies in the CMZ encompassing MIS 11 are limited to the long record of Site U1446 (Clemens et al., 2021; McGrath et al., 2021; Bhadra and Saraswat, 2022). In addition, three high-resolution speleothem records from nearby caves in China, although not within the CMZ, specifically examine MIS 11 regional monsoonal variability (Cheng et al., 2016; Zhao et al., 2019; Wang et al., 2023). An in-depth analysis of MIS 11 reveals that all these records exhibit marked dissimilarities throughout the interval, and that some lack the required temporal resolution for a robust assessment (e.g., average of ~4 kyr, Bhadra and Saraswat, 2022), which hampers the identification of a clear signal of the ISM. This study presents the first reconstruction of ISM-driven vegetation changes during MIS 11 over India's CMZ based on marine pollen analysis at Site U1446. This approach is well-established for tracking changes in the tropical forest composition, which primarily reflect variations in ISM rainfall (Clément et al., 2024). To provide unprecedented information on the mechanisms driving India's tropical vegetation and monsoon across the changing boundary conditions of MIS 11 - insolation, CO_2, and ice sheets - we also conduct a data-model comparison by analysing transient simulations performed with the LOVECLIM Earth System Model described in Yin et al. (2021).

2. Environmental setting and pollen signal

Site U1446 (19°5'N, 85°4'E) was recovered during IODP Expedition 353 "Indian Monsoon Rainfall" in the NW Bay of Bengal, offshore the Mahanadi River basin, at 1440 meter below sea level under pelagic/hemipelagic sedimentation and without turbidite disturbance (Fig. 1). This site was strategically drilled to capture the signal from the CMZ, located in central India's CMZ (Fig. 1). This zone, which receives 80-90% of its annual rainfall during the summer months (June to September, with a mean of ~250 mm/month), is representative of ISM variability across the entire Indian Peninsula as rainfall in the CMZ strongly correlates with all-India summer monsoon rainfall (Gadgil, 2003).

The ISM variability is primarily determined by the interhemispheric migrations of the Intertropical Convergence Zone (ITCZ; commonly defined as the latitude of highest precipitation) in response to the seasonal insolation cycle (e.g., Webster et al., 1998; Gadgil, 2003; Goswami and Chakravorty, 2017; Zhang and Wang, 2008; Schneider et al., 2014). The development of monsoon rainfall during the summer is due to an ITCZ shift towards the warmer northern hemisphere and an enhancement of the land-sea thermal contrast which increases the moisture supply to the continent. Besides, the ISM dynamics can be modulated by tropical atmospheric and oceanic phenomena such as the El Niño Southern Oscillation and the Indian Ocean Dipole, though their impact remains highly debated (e.g., Kumar et al., 1999; Hrudya et al., 2020; Krishnamurthy and Goswami, 2000; Goswami and An, 2023).

Vegetation distribution and composition on the Indian Peninsula are mainly influenced by the amount of annual rainfall and the duration of the dry season, both regulated by ISM changes, and to a lesser extent by the mean temperature of the coldest month (Legris, 1963; Champion and Seth, 1968; Gunnell, 1997). Notwithstanding the current prevalence of anthropogenic landscapes, the potential natural vegetation of the Indian subcontinent ranges from desert and tropical dry savannas in the interior and western areas to subtropical and tropical moist deciduous, semi-evergreen and evergreen forests in the SW and NE regions (Legris, 1963; Champion and Seth, 1968). The most humid forest type, the wet evergreen forest, is mostly located in the Western Ghats of the SW peninsula (annual rainfall >2300 $mm.yr^{-1}$), while xeric vegetation dominates the Thar Desert in the NW region (annual rainfall <500 $mm.yr^{-1}$). The Mahanadi catchment area, more specifically, encompasses four principal types of potential vegetation (Fig. 1): (1) semi-evergreen forests, found in limited coastal regions and humid lowlands of the lower Mahanadi basin under maritime influence (annual rainfall >2000 $mm.yr^{-1}$); (2) tropical moist deciduous forests, developing at higher altitudes in the basin, typically between 300 and 750 m (annual rainfall 1300 to 2000 $mm.yr^{-1}$); (3) tropical dry deciduous forests (savanna), thriving in lowland areas, mainly in the central plains of the watersheds with reduced humidity (annual rainfall 900 to 1300 $mm.yr^{-1}$); and (4) mangroves, largely influenced by edaphic factors, spreading across coastal environments, including deltaic areas, estuaries and lagoons. Site U1446 is ideally located for pollen-based vegetation reconstructions of the Mahanadi watershed due to its proximity to the river mouth and the narrow continental shelf (~25-60 km wide), which ensures efficient delivery of continental material, such as pollen grains, to the deep sea. In addition, the pollen content of marine sediments from the eastern Indian margin provides an integrated regional image of the vegetation in India's CMZ and a robust tool for reconstructing ISM-driven vegetation changes (Zorzi et al., 2015; 2022; Clément et al., 2024).

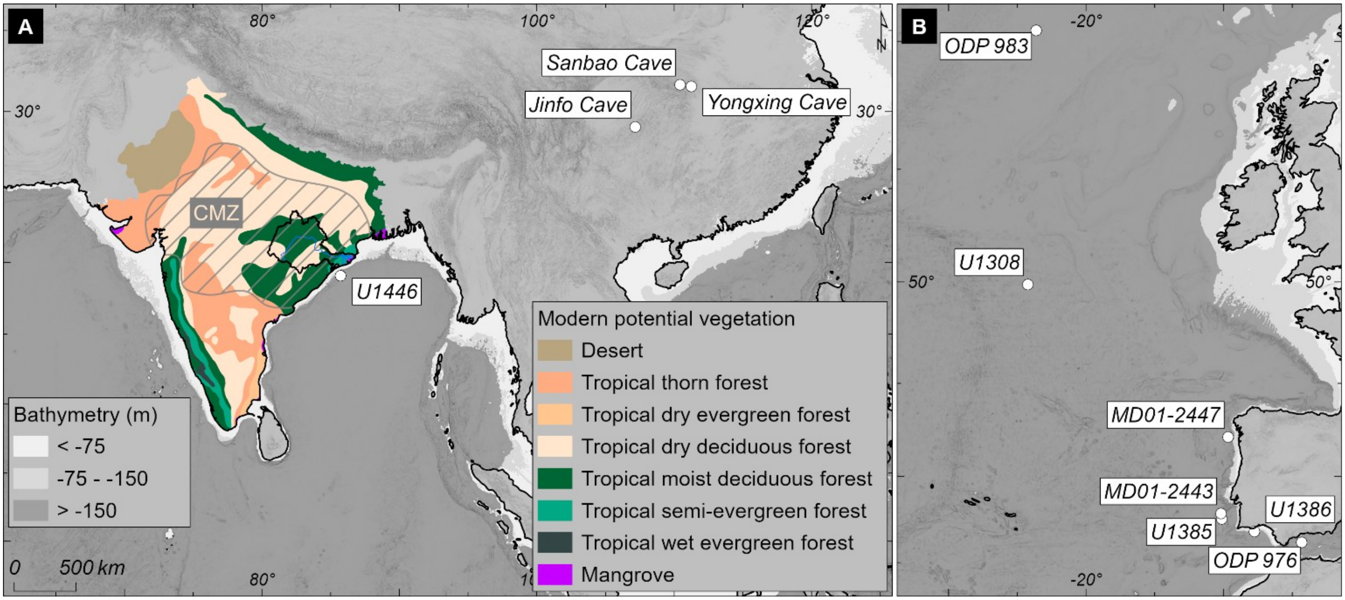

Fig. 1. A - Location of IODP Site U1446 and Chinese stalagmite records from Sanbao (Cheng et al., 2016), Jinfo (Wang et al., 2023), and Yongxing (Zhao et al., 2019) caves. Distribution of modern potential vegetation across the Indian Peninsula, with the Mahanadi catchment outlined in bold and the Core Monsoon Zone (CMZ) indicated by a striped area (adapted from Zorzi et al., 2022). B - North Atlantic records referenced in the text: ODP 976 (Sassoon et al., 2023); U1386 (Hes et al., 2022); U1385 (Oliveira et al., 2016); MD01-2443 (Tzedakis et al., 2009); MD01-2447 (Desprat et al., 2005; 2017); U1308 (Hodell et al., 2008); ODP 983 (Barker et al., 2015; 2019).

3. Methods

The original chronology of Site U1446 is based on the correlation of the benthic oxygen isotope ($\delta^{18}O_b$) record to the LR04 stack (Clemens et al., 2021). However, we constructed a new age-depth model to use a consistent chronostratigraphic framework because this study compares the Bay of Bengal record with the North Atlantic and EPICA Dome C records, all on the AICC2012 timescale (Figs. S1, S2, Table S1). We selected three tie-points between the $\delta^{18}O_b$ records from IODP Sites U1446 and U1385 spanning the period from the MIS 10 glacial maximum to the end of MIS 11c. We used the AICC2012-derived chronology developed by Nehrbass-Ahles et al. (2020) for Site U1385. Since the Iberian margin site has a hiatus at Termination V (TV), we selected two additional tie-points using the ODP 983 $\delta^{18}O_b$ record (Raymo et al., 2004; AICC2012 timescale of Barker et al. (2019)), one at the base of TV and one at the MIS 13/12 transition. We acknowledge that tuning $\delta^{18}O_b$ records from different ocean basins may introduce uncertainties of several millennia, that may vary over time (Govin et al., 2015). However, when Site U1446 chronology is transferred to the AICC2012 timescale, millennial-scale decreases in the high-frequency XRF calcium signal (Ca_{XRF}) from Site U1446, observed from MIS 10 to the end of MIS 11c and at the base of TV, align with abrupt North Atlantic warming following ice-rafted debris (IRD) events recorded at Sites ODP 983, U1385, and in the GLT_syn data (Fig. S2). Such correspondence between an increase in surface water stratification in the Bay of Bengal and an abrupt warming in the North Atlantic following a Heinrich event has been observed for the last glacial period and last Termination (Zorzi et al., 2022). In addition, this new chronology gives an age of 426 ka to the abrupt decrease in Ca_{XRF} at the beginning of TV, which is consistent with the age of the TV abrupt warming recorded in the GLT_syn record (Barker et al., 2019) and at Bàsura Cave in northern Italy at 426 ± 2 ky (Hu et al., 2024) and with the end of the millennial-scale event of weak Asian monsoon recorded at Sanbao Cave at 426 ± 1 ky (Cheng et al., 2016). The age-depth model is based on linear interpolation between control points, which gives a mean temporal resolution of 1.2 kyr between samples to the pollen record.

A total of 62 samples were taken for pollen analysis, and prepared following the methodology described in Georget et al. (2025). Sediment subsamples were processed using the standard protocol for marine samples, which includes coarse sieving (150 µm mesh), consecutive treatments with cold HCl and cold HF, and micro-sieving (5 µm mesh). Pollen analyses were performed using a Nikon light microscope at ×500 and ×1000 (oil immersion) magnification, with identification based on tropical flora atlases (Thanikaimoni, 1987; Tissot et al., 1994; Gosling et al., 2013) and reference collections from the French Institute of Pondicherry, India, and OSU OREME, France. Each sample comprised 18 to 53 pollen morphotypes to provide a reliable image of the vegetation community and its floristic diversity (McAndrews and King, 1976) and reached a total sporo-pollen sum between 142 and 247, with a main pollen sum >140 pollen grains excluding Himalayan taxa (*Alnus*, *Betula*, *Cedrus*, *Corylus, Myrica, Pinus*), aquatics and spores. Pollen percentages for terrestrial taxa were calculated from the main sum; Himalayan taxa from the main sum plus their individual counts; and aquatic and spores from the total sum (pollen + spores + indeterminables + unknowns). Results were displayed in a pollen percentage diagram drawn with the software package Psimpoll 4.25 and Pscomb 1.03 (Bennett, 2008) (Fig. S3). Major pollen zones were identified by visual inspection of percentage fluctuations in at least two ecologically distinct morphotypes (Birks and Birks, 1980) and confirmed through constrained hierarchical cluster analysis using the Euclidean distance between samples ("chclust" function from package *Rioja:* Juggins, 2009; R environment v. 3.1.1(R Core Team, 2014)) (Fig. S3).

Based on recent palynological analysis at Site U1446 (Clément et al., 2024), the interpretation of our results was supported by four main ecological groups reflecting similar annual precipitation requirements: total tropical forest, tropical deciduous forest, wet evergreen forest, grasslands and xerophytes (Legris, 1963; Champion and Seth, 1968; Bonnefille et al., 1999; Anupama et al., 2000; Barboni, 2000; Barboni and Bonnefille, 2001; Barboni et al., 2003) (Figs. 2, 3, 4, S3, Table S2). The expansion of the total tropical forest, comprising all arboreal taxa except Himalayan morphotypes, indicates higher forest cover primarily driven by intensified monsoon rainfall. In contrast, the development of graminoid grasslands, mainly represented by Poaceae, reflects a more open environment due to reduced rainfall, whereas the increase of xerophytes, mostly Amaranthaceae, Ephedraceae and *Artemisia*, suggests pronounced aridification. The tropical deciduous forest comprises species found in both dry and moist formations of the Mahanadi basin, mainly Combretaceae/Melastomataceae, *Haldina*, *Glochidion*, *Schleichera*, *Cassia*, *Holoptelea*, *Hardwickia*, and *Tectona*, which are grouped due to the indistinguishability of their pollen rain (Bonnefille et al., 1999; Barboni et al., 2003). However, a simultaneous increase of grassland and deciduous tree taxa likely suggest a wooded savanna expansion (i.e. dry deciduous forest formation). The wet evergreen forest group includes pollen morphotypes from evergreen, semi-evergreen and moist deciduous forests that thrive in wettest forest formations in India. Its most representative pollen indicators are the taxa indicative of evergreen forests, namely *Elaeocarpus, Gnetum, Mallotus, Moraceae/Urticaceae, Olea paniculata, Syzygium,* and *Trema* (Bonnefille et al., 1999; Anupama et al., 2000; Barboni, 2000; Barboni and Bonnefille, 2001; Basumatary et al., 2014; Quamar and Bera, 2015; Mehrotra et al., 2022). Given the dependence of these taxa on high precipitation levels, this group is used as the primary indicator of the ISM rainfall variability.

To decompose the time series into low-frequency (orbital-scale) and high-frequency (millennial-scale) signals, we applied a Gaussian smoothing to Site U1446 pollen data (Figs. 2a-e and 3). For that, we used the function smth.gaussian() from the R package smoother (Hamilton, 2015). The bandwidth for the kernel smoothing was chosen to provide smoothing over a window of 7 ky. This window is commonly used to separate the millennial-scale from orbital-scale changes in paleoclimate series (Barker et al., 2011, 2019). The high-frequency component was obtained by calculating the residuals between the unsmoothed and the smoothed time series. As recommended by Barker et al. (2011), a final Gaussian smoothing with a bandwidth of 0.7 ky was performed to reduce noise. Prior to data smoothing, the timeseries were interpolated using a constant step close to the first quartile of the inter-sample spacing of each original time series to avoid oversampling or underrepresentation of the high-frequency changes. Millennial-scale events of forest contraction were identified when at least one data point exceeded the threshold of one standard deviation (1σ) from the mean residual value of the wet evergreen forest percentages (Fig. 3). These significant forest contractions occurring during the glacial inception were also associated with pronounced increases in xerophytic plant percentages that surpassed 1σ of their residuals.

To evaluate the drivers of vegetation and climate variability during interglacial conditions, we compared the pollen-based reconstructions with two LOVECLIM1.3 transient simulations described in Yin et al. (2021) (Fig. 4f). The simulations span the interval from 424 to 382 ka BP, covering two precessional cycles over MIS 11. One simulation is driven by time-varying insolation (Berger and Loutre, 1991) and CO_2 (Lüthi et al., 2008); the other is driven by time-varying insolation only, with CO_2 being fixed at 280 ppmv. In both simulations, the ice-sheet configuration is prescribed at present-day conditions. LOVECLIM1.3 is an Earth system model of intermediate complexity (Goosse et al., 2010). In this study, its atmosphere (ECBilt), ocean and sea-ice (CLIO) and terrestrial biosphere (VECODE) components are interactively coupled. ECBilt is a quasi-geostrophic potential vorticity atmospheric model with 3 levels and a T21 horizontal resolution. CLIO consists of an ocean general circulation model coupled to a comprehensive thermodynamic–dynamic sea-ice model. Its horizontal resolution is 3° by 3°, and there are 20 levels in the ocean. VECODE is a reduced-form model of vegetation dynamics and of the terrestrial carbon cycle, and it simulates two plant function types, tree and grass. Vegetation fractions within a land grid cell are dictated by empirical climatic conditions, specifically annual precipitation and positive degree-days (Brovkin et al., 1997). Previous studies using transient simulations with LOVECLIM1.3 have demonstrated consistency with vegetation reconstructions from

Site U1446 for the Holocene and MIS 5e, and were further corroborated by the general circulation model HadCM3 (Clément et al., 2024).

4. Results and discussion

4.1. Indian vegetation and summer monsoon response to MIS 11 climate change

Cluster analysis of the pollen record distinguished nine pollen assemblage zones that represent major shifts in the vegetation cover and composition between 433 and 363 ka, encompassing late MIS 12, the ~56-kyr long MIS 11 and early MIS 10 (Fig. 2, and Fig. S3 and Table S2 for a summary of the main features of the pollen zones).

Site U1446 pollen record shows two intervals characterized by an open vegetation, mainly composed of grasslands and semi-arid taxa (mostly Poaceae and Amaranthaceae) that correspond to the glacial stages MIS 12, 433-426 ka, and MIS 10, 363-370 ka (Figs. 2a-e and S3, Table S2). The dominance of semi-arid steppe during these intervals indicates prevailing dry conditions and very low ISM rainfall. Cooler conditions during these glacial stages may also have favored the opening of the vegetation. However, in the tropical regions such as India, cooling is likely to have remained small compared to precipitation change. SST records from Site U1446 show temperatures that stayed above 25 °C even during the glacial maxima of the last million years (Clemens et al., 2021). Land temperatures were probably lower than ocean temperatures (Kageyama et al., 2021), although LGM climate simulations predict an annual surface temperature above 20°C and a winter temperature above 10°C in most of India (Liu et al., 2020a). Such temperatures still lie within the envelope of the hot steppe and desert bioclimatic zone (Kottek et al., 2006) suggesting that the expansion of a semi-arid steppe during glacial periods in India is more likely to be the result of changes in precipitation than temperature. In combination with climate change, the low CO_2 concentrations of the glacial periods may also have favored the expansion of open vegetation since C4 grasses are physiologically favored by reduced atmospheric CO_2 conditions (Ehleringer et al., 1997; Harrison and Prentice, 2003) but the high abundance of xerophytic plants which are C4 dicots attests to drier conditions during MIS 12 and 10.

The MIS 11 in central India, from ~426 to 370 ka, comprises three major forest phases that are interspersed with periods of more open vegetation, ranging from grasslands to semi-arid savannas (Figs. 2a-e and S3, Table S2). Based on the current relationship between vegetation distribution and precipitation in India, changes in the main ecological groups are interpreted as reflecting shifts in ISM rainfall (Clément et al., 2024, and references therein). Vegetation simulations from transient model experiments of MIS 11 show that the tree fraction is strongly correlated with annual precipitation in South Asia but has a very weak relationship with the growing degree days above 0 (Su et al., 2023). This suggests that temperature variations during MIS 11 may also have influenced vegetation in India (outside mountain ranges), but likely played a minor role. The longest, largest and most floristically diverse forest phase (tropical forest taxa reaching 32 to 58%, including *Mallotus*, *Olea paniculata*, *Cannabis/Celtis*, *Trema*, Moraceae/Urticaceae, Combretaceae/Melastomataceae, *Glochidion*, *Haldina*) occurs during the interglacial substage MIS 11c, between ~426 and 394 ka. This interval is essentially characterized by a well-developed wet evergreen forest (10-35%, mean 21%) indicating that a humid climate with increased summer monsoon rainfall persisted for approximately 32 ka. In addition, records from both tropical forest and wet evergreen forest clearly display an asymmetric "M-shaped" pattern featuring two peaks, a first one in early MIS 11c and a stronger one in the mid-MIS 11c (at ~424 and 407 ka, respectively), followed by a gradual decline from late MIS 11c to MIS 11b, between ~406 and 394 ka (Fig. 2d-e). During mid-MIS 11c, the strongest expansion of both total tropical forest and wet evergreen forest taxa (wet evergreen forest peak: 35%, mean 26%), associated with reduced abundances of tropical deciduous taxa and herbaceous plants, indicates that the summer monsoon in India reached its maximum intensity during this period of MIS 11, ~414-407 ka (Fig. 2c-e). The presence of highly moisture-demanding evergreen taxa, such as *Celtis/Cannabis, Caryota, Elaeocarpus*, *Eurya* and *Gnetum*, further supports our interpretation as they thrive in the heaviest rainfall regions of India (Fig. S3, Table S2). This wettest phase was rapidly interrupted by a major decline in the tropical forest (from 58 to 32%) and followed by a gradual contraction indicating a drying trend until the end of MIS 11c, between 406 and 394 ka, although humidity remained sufficient to sustain the wet evergreen forest (mean 15%) (Fig. 2d, e). Over this interval, the tropical deciduous forest (mainly Combretaceae/Melastomataceae, *Glochidion*, *Haldina*) and grasses largely increased in the study area, indicating an expansion of savannahs related to increasing dryness. The δD_{precip} record from Site U1446, estimated from C28 n-acid in leaf waxes and reflecting ISM circulation (McGrath et al., 2021), does not display a decline during the first forest peak (Fig. 2f). However, the isotopic minima during the second forest peak indicate intensified ISM circulation during the mid-MIS 11c, followed by a reduction through late MIS 11c, in agreement with our reconstructions.

During the late MIS 11, from ~394 to 370 ka, Site U1446 shows a gradual decline in the tropical forest with concurrent expansion of grasslands (Poaceae) and xeric elements (mostly Amaranthaceae) reflecting a long-term drying in the CMZ (Figs. 2a-e and S3, Table S2). However, fluctuations in these ecological groups also reveal superimposed ISM variability. The cold substage MIS 11b, between 394 and 388 ka, is marked by a strong increase in grasslands and xerophytes at the expense of the tropical forest (minima of tropical forest: 18% and wet evergreen forest: 1.9%), indicating drier conditions due to reduced ISM. Subsequently, during the warm stage MIS 11a (388 - 370 ka), two major phases of tropical forest expansion are identified from 388 to 380 ka and 375 to 370 ka, based on constrained hierarchical analysis of the pollen record (maxima of tropical forest: 42%, wet evergreen forest: 21%). The two forest phases are separated by a more open vegetation interval indicating a summer monsoon decrease (Fig. 2a-e and Fig. S3). These changes in vegetation are associated with the orbital-scale variability, as shown by the 7-ky Gaussian-smoothed data (Fig. 2a-d). Both forest expansions during MIS 11a coincide with decreases in δD values (Fig. 2f). However, the δD_{precip} does not record the distinct amplitudes of these peaks likely due to its low time resolution as well as the influence of multiple factors affecting isotopic signatures, such as atmospheric transport pathways, source regions and interactions with vegetation (McGrath et al., 2021; Clément et al., 2024).

Superimposed on the declining percentages of the total tropical forest and wet evergreen forest, indicating gradual aridification through MIS 11, Site U1446 also records millennial-scale changes in the Indian vegetation (Figs. 2d, e and 3). Based on the criteria outlined in Section 3 (Fig. 3), we identified four major tropical forest shifts (labelled Forest event Fe-1 to Fe-4) that correspond to events of significant contraction of the wet evergreen forest. These forest events reflect abrupt changes to drier conditions likely driven by ISM weakening. The first and most dramatic forest contraction, recorded at ~406 ka, is marked by a high-amplitude and abrupt decrease in the tropical forest (22.3% in ~1.6 kyr) mainly due to a decline of the wet evergreen forest at the expense of grasses (Poaceae) (Figs. 2b-e and 3). After Fe-1, the progressive decrease in tropical forest during late MIS 11 is interrupted by three significant forest contraction events, events Fe-2, -3, and -4, centered at ~387.7 ka, 383.3 ka and 374.6 ka, respectively (Figs. 2 and 3). Each event is also marked by large increases in xerophyte plants (maxima >21%) and concurrent declines in wet evergreen elements (minima <4%), indicating the expansion of semi-arid savannas in the studied region, which reflects the most severe drought conditions and reduced ISM during MIS 11. These high-intensity events are rapidly followed by a sharp increase in tropical forest taxa with wet evergreen elements (13% for Fe-2/Fe-3 and 23% for Fe-4, within 0.6-1 kyr), indicating abrupt transitions to wetter conditions driven by an intensified ISM.

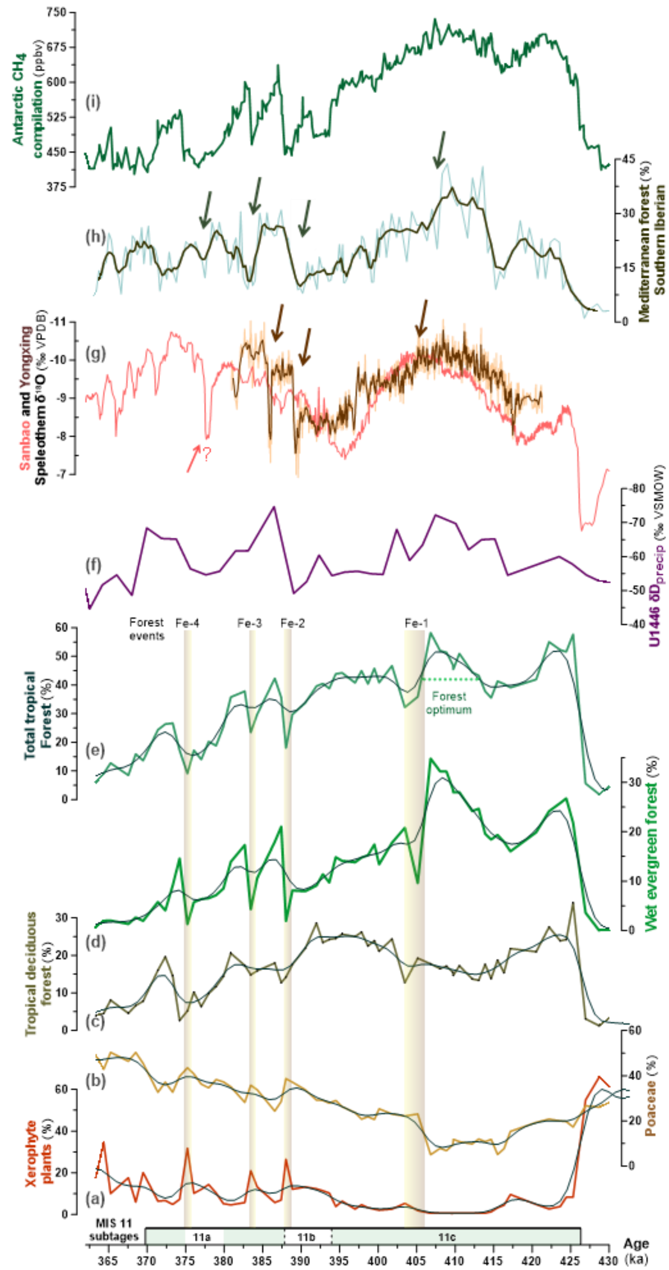

Fig. 2. MIS 11 ISM-driven vegetation changes at Site U1446 - represented by the percentages of the main ecological groups/taxa with black lines representing the orbital-scale pattern extracted through a 7 ky-Gaussian smoothing filter (a) xerophyte plants, (b) Poaceae, (c) tropical deciduous forest, (d) wet evergreen forest, and (e) total tropical forest - in the context of changes in (f) U1446 δD_{precip} (McGrath et al., 2021; lighter values reflect precipitation amount and moisture-source/transport changes), (g) Chinese speleothem $\delta^{18}O$ from the Sanbao (Cheng et al., 2016) and Yongxing caves (Zhao et al., 2019), (h) Southern Iberian Mediterranean forest from Site U1386 and U1385 (bold line – 3 point moving average,

chronology derived from LR04) (Oliveira et al., 2016; Hes et al., 2022) and (i) CH_4 concentrations from the Antarctica EPICA Dome C ice core, AICC2012 chronology (Nehrbass-Ahles et al., 2020). MIS 11 substages are indicated at the bottom, with pollen zones distinguishing three forest expansion phases marked by green bands during MIS 11c and 11a, interspersed with phases of more open vegetation during MIS 11b and mid-MIS 11a. Forest events (Fe-1 to -4) are depicted by brown bands indicating forest contractions/ISM weakening. Arrows in (g) and (h) denote potential concurrent millennial-scale events.

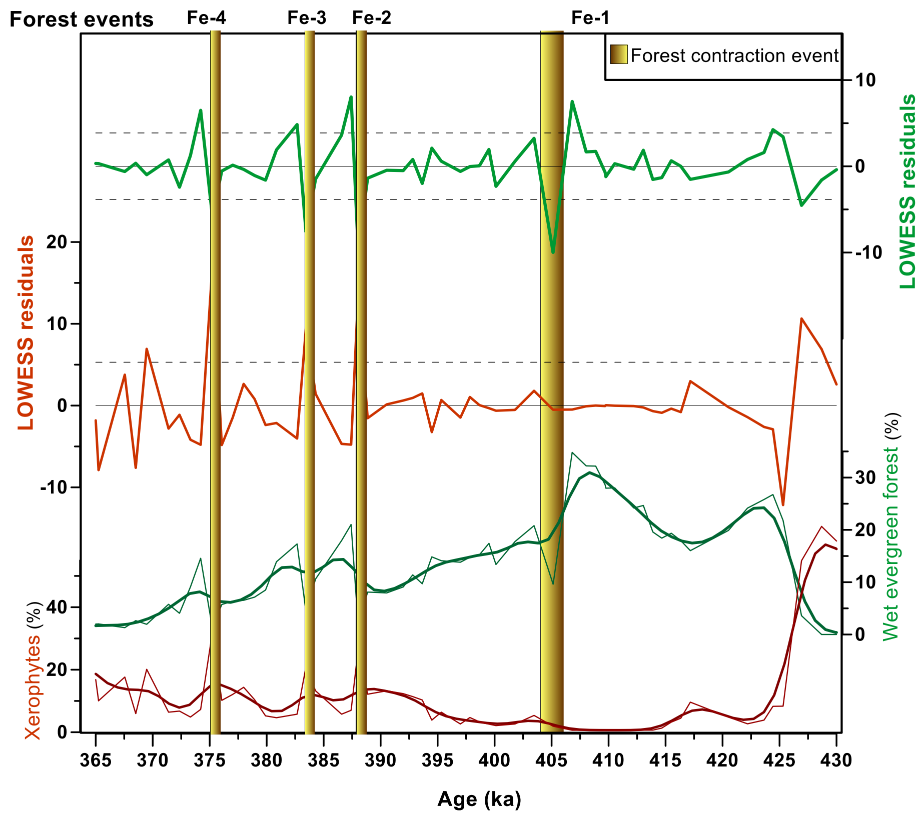

Fig. 3. Pollen percentage curves of the xerophyte plants and the wet evergreen forest (bottom panel) along with the respective Gaussian smoothing filter (7 ky-Gaussian filter, bold line) and the residuals (top panel) during MIS 11. Millennial-scale forest contraction events (brown bands) were identified when at least one sample of the model residuals exceeded the threshold of one standard deviation (± 1σ). Significant forest contractions occurring during the glacial inception were also concomitant with pronounced increases in xerophyte taxa percentages surpassing 1σ of their residual values, and were followed by significant expansions of wet evergreen tropical forest taxa.

4.2 Orbital-scale changes

Site U1446 pollen-based reconstructions reveal a sharp transition from a semi-arid savanna in late MIS 12 to established tropical forests in MIS 11 (tropical forest: increase from 2 to 58%, Fig. 2e), indicating a rapid response to an extreme hydroclimatic change. These results indicate that the vegetation in the CMZ responded to a steep northward shift of the ITCZ and associated intensification of the South Asian monsoon rainfall across the MIS 12/11 transition, in line with observations from the long records of the same site (Clemens et al., 2021), as well as from southern Bay of Bengal (Bolton et al., 2013; Gebregiorgis et al., 2018) and East Asian speleothems (Cheng et al., 2016; Wang et al., 2023) (Fig. 2f, g).

During the interglacial MIS 11c, the pollen record from Site U1446 provides evidence for a large expansion of the tropical forest in India's CMZ, reflecting a sustained interval of increased ISM activity (Fig. 2d, e). This forest expansion aligns with findings from previous palynological studies across the northern hemisphere documenting maximum vegetation cover and biodiversity during MIS 11c attributed to enhanced warmth and/or precipitation (e.g., Greenland: de Vernal and Hillaire-Marcel 2008; NE Russia: Melles et al., 2012; Siberia: Prokopenko et al., 2010; Central Asia: Xiao et al., 2010; Zhao et al., 2020; Hayashi et al., 2021; Europe: Candy et al., 2014; 2024 and references therein; North America: Fawcett et al., 2011; South America: Torres et al., 2013; NW Africa: Dupont and Agwu, 1992; Dupont et al., 1998; global data-model comparison: Kleinen et al., 2014). Our results further reveal that MIS 11c exhibits two consecutive increases in tropical forest, the first one in early MIS 11c and the second one, more pronounced in mid-MIS 11c, revealing an interval of intense monsoon activity between ~414 and 407 ka (Fig. 2e). Such tripartite division of MIS 11c, classically referred as asymmetric "M-shaped" structure with an optimum in the mid-MIS 11c, is one of the key characteristics of this interglacial, being well-represented in records from Antarctic ice cores, global sea-level/ice volume, and both terrestrial and marine sequences across the northern hemisphere (e.g., Lisiecki and Raymo, 2005; Jouzel et al., 2007; Candy et al., 2014; 2024; Grant et al., 2014; Kandiano et al., 2017; Nehrbass-Ahles et al., 2020; Tzedakis et al., 2022 and references therein). However, the pattern and duration of each phase are heavily dependent on the archive and climate indicators under investigation. At close inspection, the asymmetric "M" pattern of our forest records closely aligns, within age uncertainties, with the high-resolution southern European marine pollen sequences from the Iberian margin (Desprat et al., 2005; 2017; Tzedakis et al. 2009; Oliveira et al., 2016; Hes et al., 2022) (Fig. 2h), and the record of atmospheric methane concentrations (CH_4 hereafter) from the EPICA Dome C Antarctic ice core (Nehrbass-Ahles et al., 2020) (Fig. 2i). We propose that these concomitant changes in the vegetation and hydroclimate in the low and mid-latitudes reflect shifts in the ITCZ position that, in turn, have a prominent imprint on the CH_4 record. Such suggestion is supported by the ITCZ's well-recognized role in regulating past and present-day tropical monsoon systems and its impact on the extent of tropical wetlands, one of the largest natural sources of this greenhouse gas (e.g., Guo et al., 2012; Kirschke et al., 2013; Schneider et al., 2014; Bock et al., 2017). Secondary sources of CH_4 during MIS 11c might have included boreal wetland expansion and/or permafrost thawing due to warmer conditions, as suggested by speleothem and paleotemperature data (Melles et al., 2012; Vaks et al., 2013, 2020; Batchelor et al., 2024). Unlike proxy records from low and mid-latitudes, the northern latitude records, such as Lake El'gygytgyn in Siberia (Melles et al., 2012), show strong warming from the beginning of MIS 11c, which resembles the slight difference between the two CH_4 maxima (Fig. 2i). This similarity suggests that boreal regions may have also contributed to methane emissions during the early phase of MIS 11c, even though tropical wetlands remained the dominant source throughout this substage. Tzedakis et al. (2009) first attempted to link coupled southern European vegetation and CH_4 changes to shifts in the ITCZ, to reveal the potential impact of low-latitude emissions on CH_4 over the past 800 ka. So far, confirming this hypothesis has been challenging due to the lack of detailed records of the low-latitude hydrological cycle for comparison with mid-latitude data. Subsequent studies (Nehrbass-Ahles et al., 2020; Tzedakis et al., 2022) have used the Sanbao speleothem record as an indicator of low-latitude hydroclimate and tropical wetland extent during MIS 11. The Chinese speleothem isotopic signals, used to reconstruct the East Asian summer monsoon, effectively bear the tripartite division of MIS 11c with minimal isotopic values occurring during the mid-MIS 11c (Cheng et al., 2016; Zhao et al., 2019; Wang et al., 2023), even though age offsets and variability among individual speleothem records are noticeable (Fig. 2g). Site U1446 pollen record thus provides evidence for variations of monsoon intensity within the Indian summer monsoon domain during the MIS 11 interglacial period further supporting Tzedakis et al. (2009)'s hypothesis for MIS 11.

During the stadial MIS 11b, Site U1446 pollen record indicates an expansion of a semi-arid savannah reflecting reduced summer monsoon rainfall. During the interstadial MIS 11a, the two intervals of forest expansion (388-380 ka and 375-370 ka), with higher values of total forest and wet evergreen elements during the first one, suggest two orbital-scale increases in summer monsoon in India of decreasing intensity. Variations in CH_4 concentrations during MIS 11b follow similar orbital-scale pattern (Fig. 2d, e, i). On a regional scale, monsoon activity also decreased in East Asia during MIS 11b and increased during MIS 11a intervals, as in the Indian summer monsoon domain (Cheng et al., 2016; Zhao et al., 2019; Wang et al., 2023) (Fig. 2g). However, the isotopic values exhibited by the Jinfuo and Sanbao cave records during MIS 11a are as negative as during MIS 11c, which would suggest that the East Asian monsoon reach similar intensity, which contrast with markedly lower CH_4 concentrations and extent of tropical forest in India during MIS 11a. A recent study, based on a loess microcodium $\delta^{18}O$ record from East Asia and modelling experiments, also showed, in contrast to the Chinese speleothem records, that there was a variable magnitude of summer monsoon precipitation increase during precession minima of the last 400 ky, reflecting the glacial-interglacial variability (Zhang et al., 2025). Moisture source and transport pathway can also affect the $\delta^{18}O$ calcite signal (e.g., Liu et al., 2020b). Heterogenous response of the different subsystems of the Asian summer monsoon may also be involved to explain the different signal of the speleothem records compared to Site U1446 record. Palaeoclimate profiles of the northern hemisphere largely mark MIS 11b as cooler, while MIS 11a presents two orbital-scale warmings, with the first one having a larger amplitude (e.g., Fawcett et al., 2011; Candy et al., 2014 and references therein; Grant et al., 2014; Nehrbass-Ahles et al., 2020; Sassoon et al., 2023). We infer that, akin to MIS 11c, the remarkable correspondence between low vegetation and CH_4 changes during MIS 11b and 11a (Fig. 2e, i) mirror variations in the hydrological cycle that are primarily controlled by the ITCZ's mean position in response to the orbital-scale climate changes.

4.3 Millennial-scale variability

The dramatic forest contraction Fe-1 occurs at ~406 ka during the full interglacial conditions of MIS 11c (Figs. 2 and 4). This abrupt savannization in India's CMZ with no subsequent forest recovery is likely related to a millennial-scale weak monsoon event. On a regional scale, an analogous abrupt event is only detected by the higher-resolution Chinese speleothem $\delta^{18}O$ record from Yongxing Cave (Zhao et al., 2019) (Fig. 2g). Within the chronological uncertainties, this event may coincide with an abrupt cold and dry event well documented in marine pollen sequences off southern Europe where it abruptly marks the end of the MIS 11c optimum with no later return to interglacial levels (Desprat et al., 2005, 2017; Tzedakis et al., 2009; Oliveira et al., 2016; Sassoon et al., 2023) (Fig. 2h). Strikingly, unlike the sharp vegetation contractions in India and Europe, the CH_4 record only shows a slight decline (Fig. 2i). These observations suggest that whilst tropical monsoon variability subtly influenced CH_4 emissions during this period, other sources may have played a larger role in the methane budget. Potential sources that warrant further study (e.g., Singarayer et al., 2011; Baumgartner et al., 2012; Guo et al., 2012) include high-latitude sources (wetland expansion, thawing permafrost, thermokarst lakes) driven by the warm conditions in boreal regions throughout MIS 11c, as well as increased emissions from tropical regions in the southern hemisphere. This weak monsoon event at the end of the MIS11c optimum (~406 ka) occurs during an orbital-scale decrease in boreal insolation, low ice volume conditions and high and stable CO_2 concentrations (Fig. 4e, g-i). We propose that this event may be linked to a well-documented abrupt event in southern Europe (Fig. 2h), (event U1385-11-fe-1 occurring at 408 ka on Site U1385 LR04 chronology (Oliveira et al., 2016), but at 406 ka when the Site U1385 age is transferred to the AICC2012 chronology), which has been associated with increased aridity caused by a persistent positive mode of the North Atlantic Oscillation (Oliveira et al., 2016; Kousis et al., 2018). This correspondence between low and mid-latitude regions suggests a common response to atmospheric circulation changes, either independently or via teleconnections, that resulted in dry conditions in both regions. Given the current lack of a statistically significant link between the North Atlantic Oscillation and the ISM (Brönnimann, 2007), it is more likely that the co-occurrence of dry events in southern Europe and India is related to an atmospheric pattern resembling the El Niño–Southern Oscillation (ENSO). Recognized as one of the most important global climate patterns, this coupled ocean-atmosphere mode has a strong impact on the ISM via changes in the Walker and regional monsoon Hadley circulation patterns (e.g., Webster et al., 1998; Krishnamurthy et al., 2000; Gadgil et al., 2007; Wang et al., 2013; Goswami and An, 2023). It exhibits two distinct phases, El Niño and La Niña, with El Niño phases typically associated with reduced ISM rainfall, while La Niña phases correspond to enhanced monsoon activity. Therefore, the Fe-1 event might have been driven by a shift to a prolonged or more frequent El Niño-like state. This shift would have weakened the ISM, as proposed for Holocene weak monsoon events in Central India (Prasad et al., 2014; Riedel et al., 2021), ultimately causing a tropical forest decline. In line with our suggestion of a common link, both observational and modelling studies indicate that ENSO also affects the circulation in the North Atlantic–European regions (Brönnimann, 2007). However, the influence of ENSO on European climate, as well as the mechanisms involved, remains debated. One possible explanation for the common expression of dry conditions in India and southern Europe may involve the influence of North Atlantic circulation changes on large-scale atmospheric patterns. Although the high-resolution benthic $\delta^{13}C$ record from Site U1385 does not provide clear evidence for an AMOC reduction during the ~406 ka event, intra-interglacial AMOC instability has been documented throughout MIS 11c in the northern North Atlantic (Galaasen et al., 2020). In this context, some model experiments suggest that AMOC weakening can favour a more El Niño-like state by inducing a southward displacement of the ITCZ and modifying tropical Atlantic SST gradients, which may in turn affect the equatorial Pacific thermocline through atmospheric teleconnections (Timmermann et al., 2007; Dong and Sutton, 2007). Nevertheless, the ENSO response to AMOC weakening is model-dependent, likely reflecting the difficulty of accurately simulating the tropical Pacific coupled ocean–atmosphere system (Pausata et al., 2015).

After the MIS 11c interglacial, when atmospheric CO_2 was lower and ice volume substantially increased, Site U1446 records three abrupt contractions of the tropical forest (Fe-2, -3, and -4), suggesting millennial-scale events of monsoon rainfall reduction in India, occurring during MIS 11b at ~387.7 ka, and during MIS 11a at ~383.3 ka interrupting the first major forest expansion, and at ~374.6 ka (Figs. 2d, e and 4e). The East Asian speleothems also record millennial-scale variability during the late MIS 11 (Fig. 2g). The high-resolution record from the Yongxing cave (Zhao et al., 2019), which extends only to early MIS 11a, captures two abrupt events of increased $\delta^{18}O_{calcite}$ that may relate to the events Fe-2 and Fe-3. The speleothem from Jinfo cave (Wang et al., 2023), located in southern China, records a series of weak monsoon events that may correspond to three episodes of reduced ISM detected in India within the dating uncertainties. The lower-resolution $\delta^{18}O$ profile from Sanbao cave (Cheng et al., 2016) clearly records only the youngest event, Fe-4, although two previous subtle decreases in $\delta^{18}O$ have been associated with weak monsoon events recorded at Jinfo cave (Wang et al., 2023) that correlate with the events Fe-2 and Fe-3. These differences in speleothems $\delta^{18}O$ signatures may stem from differences in-cave processes (e.g., dripwater hydrology, carbonate dissolution, fractionation) and speleothem growth dynamics contributing to the final isotopic composition (Fairchild and Baker, 2012; Hu et al., 2019). Despite chronological discrepancies, the weak monsoon events recorded at Jinfo cave have been linked to the cold North Atlantic events and associated AMOC changes (Wang et al., 2023). In our Indian vegetation-monsoon record based on marine stratigraphy, the concordance of episodes of increased aridity in India and cooling events in the North Atlantic and adjacent continent appears clearer (Fig. 4a-c, e). Similar to Site U1446, pollen records from the northern hemisphere mid-latitudes generally show an abrupt forest decrease during MIS 11b, and two other millennial-scale forest reductions during MIS 11a indicating shifts to cooler/drier conditions (Oliveira et al., 2016; Desprat et al., 2005; Sassoon et al., 2023) (Fig. 2h). In the North Atlantic, these prominent cooling events are largely documented and frequently recognized as Heinrich-type events. They have been attributed to disruptions in the AMOC caused by iceberg discharges (e.g., Oppo et al., 1998; Stein et al., 2009; Prokopenko et al., 2010; Rodrigues et al., 2011; Candy et al., 2014; Barker et al., 2015; 2019; Oliveira et al., 2016; Kousis et al., 2018; Hodell et al., 2023; Sassoon et al., 2023), as evidenced by concurrent reductions in Site U1385 $\delta^{13}C$ values and peaks in Ice-Rafted Detritus (Fig. 4a-c). We propose that during the late MIS 11, when ice volume became large enough to generate AMOC instabilities, i.e., when the $\delta^{18}O_b$ threshold of 3.5‰ was exceeded in North Atlantic records (McManus et al., 1999; Barker et al., 2015), abrupt North Atlantic cold events induced a southward shift of the ITCZ and consequent millennial-scale reductions in the summer monsoon and wet evergreen forest in India. There is a remarkable correspondence between the low-latitude vegetation and CH_4 millennial-scale changes during

MIS 11b and 11a (Fig. 4d, e), likely mirroring variations in the hydrological cycle that are primarily controlled by the ITCZ's mean position. The impact of millennial-scale North Atlantic variability on the ITCZ and, more broadly, on the tropical hydrological cycle has been shown in previous proxy and model studies of the last glacial period (e.g., Marzin et al., 2013; Mohtadi et al., 2014; Dutt et al., 2015; Ota et al., 2022; Zorzi et al., 2022). This study highlights the important role of ice sheet dynamics on the millennial-scale variability of the South Asian summer monsoon during periods of intermediate ice volume, beyond the last glacial period.

Each of the forest contractions marking the late MIS 11 is followed by a sharp increase in tropical forest dominated by wet evergreen elements (13% for Fe-2 and Fe-3 and 23% for Fe-4, occurring in 0.6-1 kyr) suggesting an abrupt intensification of ISM rainfall (Fig. 2d, e), likely associated with an ITCZ northward shift. These events all strikingly match, within age uncertainties, with abrupt forest expansion in southern Europe and warming in the North Atlantic, as indicated by Site U1385 pollen record and Site ODP 983 foraminifera record (Figs. 2 and 4). In the millennial-scale component of the synthetic Greenland temperature record of Barker et al. (2011; 2019), these three events correspond to Dansgaard-Oeschger-like warming events (Fig. 4d). In addition, they all appear to coincide with the abrupt carbon dioxide jumps and methane rises as identified by Nehrbass-Ahles et al. (2020) from the highest resolution record of CO_2 and CH_4 from the Antarctic ice core (Fig. 4d, h). Nehrbass-Ahles et al. (2020) proposed that the sharp rises in CO_2 and CH_4 are linked to Dansgaard-Oeschger-like warming events driven by sudden AMOC intensifications, as inferred from centennial-scale benthic $\delta^{13}C$ records, such as those from Iberian Site U1385 (Fig. 4c). AMOC strengthening would have enhanced heat transport to the northern hemisphere, triggering a northward shift of the ITCZ and a significant increase of low-latitude wetlands and CH_4 emissions, as corroborated by our findings. It is noteworthy that Nehrbass-Ahles et al. (2020) used the record from Sanbao cave to document the shifts in ITCZ from which the methane increases may have originate, although as noted above, most of the MIS 11 millennial-scale changes in this speleothem record are unclear (Fig. 2g). Hence, Site U1446 pollen record provides the first clear evidence for a rapid northward shift of the ITCZ and intensification of the summer monsoon, which could have enabled the necessary expansion of wetlands in tropical regions to sustain the three sharp rises in CH_4 documented for the late MIS 11.

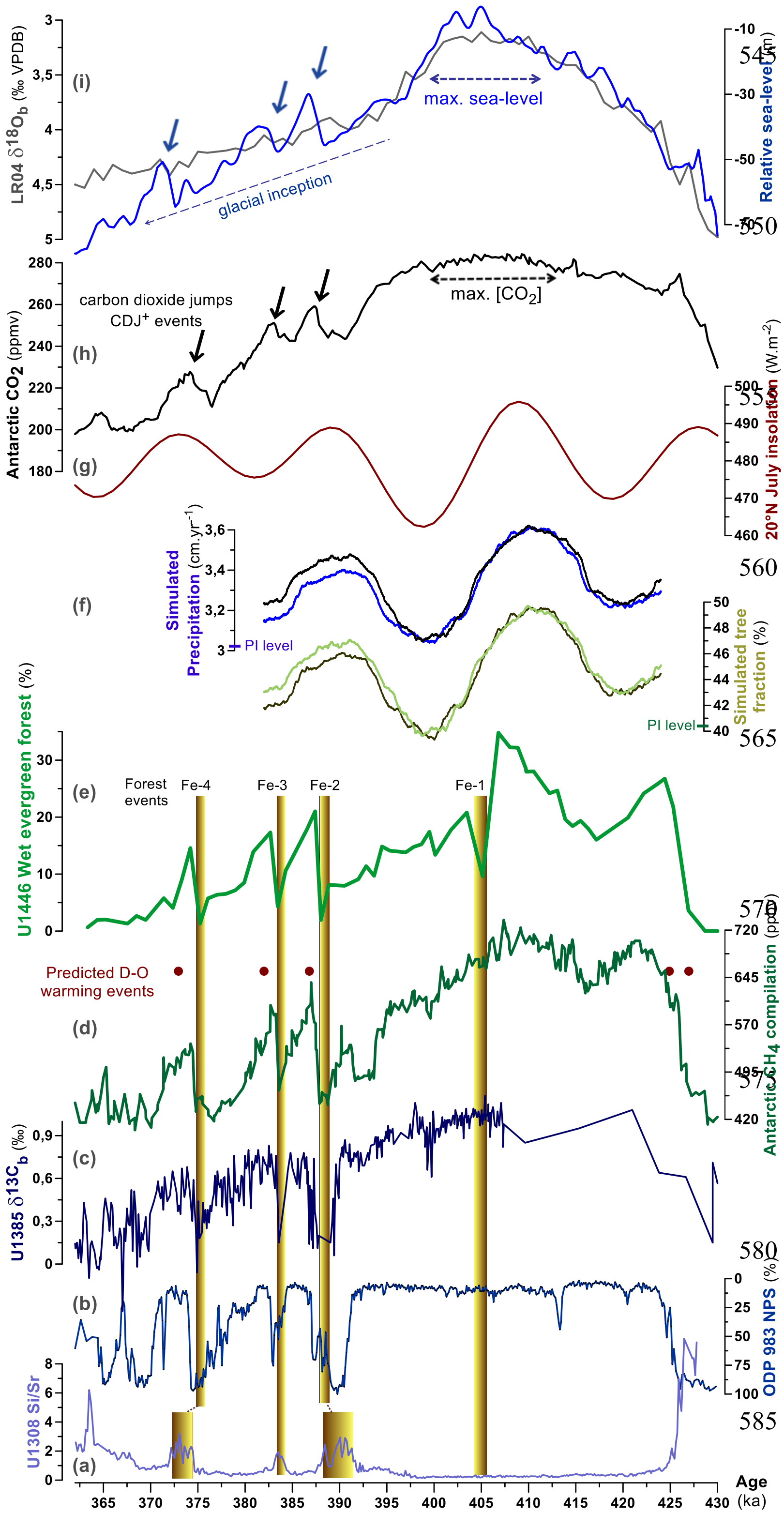
LR04 δ18Ob (‰ VPDB)
Relative sea-level (m)
(i)
max. sea-level
glacial inception
Antarctic CO2 (ppmv)
carbon dioxide jumps
CDJ+ events
max. [CO2]
(h)
(g)
20°N July insolation (W.m-2)
Simulated Precipitation (cm.yr-1)
PI level
(f)
Simulated tree fraction (%)
PI level
U1446 Wet evergreen forest (%)
(e)
Forest events
Fe-4
Fe-3
Fe-2
Fe-1
Predicted D-O warming events
(d)
Antarctic CH4 compilation (ppbv)
U1385 δ13Cb (‰)
(c)
(b)
ODP 983 NPS (%)
U1308 Si/Sr
(a)
Age (ka)

Fig. 4. MIS 11 drivers of ISM-driven vegetation variability on orbital and millennial timescales. North Atlantic changes: (a) meltwater discharges inferred from Si/Sr of Site U1308 (Hodell et al., 2008), b) ODP Site 983 polar planktic foraminifera (Barker et al., 2015; 2019), and (c) $\delta^{13}C$ from Site U1385 indicative of AMOC changes (Nehrbass-Ahles et al., 2020). (d) CH_4 record (Nehrbass-Ahles et al., 2020) with red dots denoting predicted Dansgaard-Oeschger (D-O) warming events (Barker et al., 2011). U1446 data: (e) Percentage of the wet evergreen forest with forest contraction events (Fe-1 to -4) (this study) and (f) LOVECLIM1.3 simulations averaged over the Indian CMZ (17°-27.5° N, 67.5°-90° E) for the tree fraction and annual precipitation (this study) with time-varying insolation and CO_2, and with fixed CO_2 at 280 ppmv (black line). Primary forcings: (g) July 21 insolation at 20°N (Berger and Loutre, 1991), with the pre-industrial level indicated, (h) CO_2 concentrations from EDC Antarctic ice core, arrows mark abrupt CDJ^+ (carbon dioxide jumps) coinciding with significant CH_4 increases (Nehrbass-Ahles et al., 2020) and (i) Relative sea-level from the Red Sea (Grant et al., 2014) and $\delta^{18}O_{benthic}$ from the LR04 (Lisiecki and Raymo, 2005).

4.4 Interplay of forcings behind the ISM-induced vegetation changes

To understand the mechanisms driving the changes in the CMZ of India across the changing boundary conditions of MIS 11, we compare the wet evergreen forest record with primary forcings - insolation, CO_2, and ice volume - as well as with records from the mid- to high-latitude regions of the northern hemisphere (Figs. 2 and 4).

During the early and mid-MIS 11c, both the pattern and amplitude of the wet evergreen forest record track the precession-driven summer insolation at 20°N (Fig. 4e, g). The ISM strengthens at the two insolation maxima (precession minima at 409 and 428 ka), reaching its optimum at ~407 ka, nearly in phase with the second, strongest MIS 11 insolation peak, and weakens during at the intervening insolation minima (precession maximum at 419 ka). In contrast, the changes in forest and summer monsoon do not parallel the CO_2 concentration and ice volume variations of MIS 11c which do not present the same tripartite division but a rather a regular sea-level rise until the mid-MIS 11c and high values of atmospheric CO_2 concentrations from the early MIS 11c (Fig. 4e, h, i). In addition, high levels of CO_2 concentrations (> 270 ppm) persist almost until the end of MIS 11c, well beyond the mid-MIS 11c ISM optimum while the wet evergreen forest gradually declines in tandem with decreasing summer insolation (Fig. 4e, g, h). These observations clearly highlight the dominant role of insolation forcing in driving interglacial ISM–vegetation variability through its influence on the location of the ITCZ and moisture transport to the continent (e.g., Prell and Kutzbach, 1992; Kutzbach et al., 2008; Cheng et al., 2016; Schneider et al., 2014; Mohtadi et al., 2016; Gadgil, 2018; Jalihal et al., 2019). Maxima in boreal summer insolation would have strengthened the thermal contrast between the Indian peninsula and the equatorial Indian Ocean, leading to intensified ISM rainfall via moisture transport from the Indian Ocean and Walker-type circulation anomalies. This is in agreement with previous work demonstrating that, during interglacial periods, CO_2 concentrations above ~250 ppm have a negligible impact on the vegetation dynamics in India's CMZ and insolation is the dominant driver of vegetation and summer monsoon precipitation in this region (Clément et al., 2024). Conversely, during the second part of MIS 11, long-term changes in wet evergreen forest diverge from insolation trends and vary in concert with CO_2 and sea level/ice volume reconstructions (Fig. 4e, g-i). These observations indicate that while the impact of boreal summer insolation dominates during MIS 11c interglacial conditions, CO_2 and ice-sheet dynamics become the primary drivers during the glacial inception, overriding the influence of insolation. Lower atmospheric CO_2 concentrations during the late MIS 11 likely favored the development of C4 grasses (Ehleringer et al., 1997; Cerling et al., 1998), which would have also contributed to reduced evaporation at low latitudes due to the radiative properties of this greenhouse gas. In addition, larger northern hemisphere ice sheets probably decreased atmospheric humidity and its transport to the Indian peninsula, as well as triggered a southward shift of the ITCZ (Lyu et al., 2021). As observed for the LGM, this shift would have led to increased aridity (e.g., Chiang and Bitz, 2005; Marzin et al., 2013; McGee et al., 2014) and a consequent reduction in forest cover in the CMZ (Zorzi et al., 2022).

Taken together, our MIS 11 results from India's CMZ do not support the "zero phase" hypothesis which suggests that the ISM variability is merely controlled by precession-paced boreal summer insolation (e.g., Prell and Kutzbach, 1992; Kathayat et al., 2016; Zhang et al., 2019); nor do they align with the view that it is solely driven by ice-sheet dynamics and/or CO_2 forcing (Caley et al., 2011; Bolton et al., 2013; Gebregiorgis et al., 2018; McGrath et al., 2021; Clemens et al., 2021). Instead, this work suggests that the controls of the coupled ISM-vegetation variability during MIS 11 are more complex and their predominant role likely depends on the varying baseline climate conditions (insolation, CO_2 and ice-sheets). To ensure the robustness of these conclusions we analysed LOVECLIM transient simulations forced by time-varying insolation and CO_2, as described in section 3. These experiments (Fig. 4f) and linear regression analysis (Table S3) indicate that precipitation is the primary factor explaining the simulated tree fraction over the CMZ, with surface air temperature playing a minor role, consistent with the model simulations by Sun et al. (2022). In agreement with the pollen data, both the simulated tree fraction and precipitation follow insolation rather than CO_2 changes during MIS 11c (Fig. 4f, h). This divergence is particularly obvious during the CO_2 plateau in late MIS 11c, where both simulated variables decline gradually in response to decreasing boreal summer insolation. These results are in line with previous studies demonstrating that the interglacial tree fraction over the northern tropical-subtropical regions including the Indian CMZ region, is primarily influenced by precession, while CO_2 has a minor effect (Yin and Berger, 2012; Su et al., 2022; Clément et al., 2024). Yet, in contrast to Site U1446 pollen data, the simulated tree fraction and precipitation continue to follow insolation trends across MIS 11b and early MIS 11a (Fig. 4e, f). These mismatches likely stem from the lack of ice-sheet forcing and related freshwater flux in the simulations, as suggested by data-model comparisons from the mid-latitudes (Oliveira et al., 2018). The absence of dynamical ice sheets in the model would lead to an underrepresentation of millennial-scale variability and its interactions with orbital-scale changes, which might also account for the data-model discrepancies. These millennial-orbital scale climate interactions could explain the observed abrupt forest decline during MIS 11c (Fe-1) and the subsequent forest events at the end of MIS 11b/transition to MIS 11a (Fe-2), which are inconsistent with insolation changes (Figs. 2 and 4).

Notably, according to our simulations, conditions in the CMZ of India were considerably wetter and more forested at the climate optimum of MIS 11c than during the pre-industrial period (Fig. 4f), due to much higher boreal summer insolation (Fig. 4g). These results highlight the importance of further studying MIS 11 and the responses of terrestrial ecosystems in ISMaffected regions, as they may offer valuable analogues for 21st-century climate conditions, where an intensified ISM is expected to lead to denser and greener vegetation, with deciduous trees potentially replacing grassland (Sharmila et al., 2015; Liu et al., 2020c; Varghese et al., 2020; Katzenberger et al., 2021).

5. Conclusions

India's tropical vegetation and summer monsoon changes during MIS 11, a potential analogue of the Holocene, are investigated through a new pollen record from Site U1446 in the Bay of Bengal, and their comparison with model simulations. The strong correspondence between our tropical forest record, southern European vegetation, and CH_4 concentrations suggests that the link between low and mid-latitudes was mediated by shifts in the ITCZ's mean position and reflected in the CH_4 levels, largely controlled by low-latitude wetland emissions. We reveal that the dominant forcings of coupled ISM-vegetation variability, primarily driven by ITCZ shifts, depended on the interplay between the boundary conditions through MIS 11 - insolation, CO_2, and ice sheets - as well as orbital and millennial-scale changes related to the AMOC.

During interglacial MIS 11c, our forest records mirror changes in CH_4, indicating that the shifts in the ITCZ closely track the precession-paced boreal summer insolation. Unprecedented evidence shows that ISM and forest maxima occur in phase with the strongest insolation peak of MIS 11c but precede the maxima in CO_2 and sea level, demonstrating the dominant influence of insolation forcing on ISM-vegetation variability under warm and high atmospheric CO_2 background conditions. This forest optimum is interrupted by the most prominent forest contraction, ~406 ka, suggesting that extreme reductions in ISM can also occur during globally warm conditions. An equal impact is observed in terrestrial ecosystems at mid-latitudes, despite no equivalent change in the marine realm or in the CH_4 record. While the drivers behind this event remain unclear, we propose that future research should prioritize atmospheric circulation patterns affecting both low and mid-latitude regions, with a specific focus on ENSO.

The second part of MIS 11 is marked by ISM-vegetation changes that diverge from insolation trends and align with CO_2 and sea level/ice volume reconstructions, revealing that atmospheric CO_2 and high-latitude ice-sheet dynamics become the primary drivers during substages MIS 11b and 11a. Moreover, superimposed on the long-term trends, our record captures three major ISM-driven forest events, at ~387.7 ka, 383.3 ka, and 374.6 ka, indicating that interactions between long-term and millennial-scale changes are a prominent feature during the glacial inception of MIS 11. Abrupt forest contractions indicate a southward ITCZ shift linked to high-latitude processes involving ice rafting, North Atlantic cooling and AMOC reductions, whereas forest expansions suggest a rapid ITCZ poleward shift associated with CH_4 overshoots and invigorated AMOC activity.

The comparison of Site U1446 pollen-based reconstructions with transient experiments using time-varying insolation and CO_2 reveals that the boreal summer insolation is the primary driver of climate dynamics during MIS 11c. The mismatch observed between the pollen data and model outputs during MIS 11b and early MIS 11a emphasizes the need to incorporate ice sheet dynamics into model simulations to investigate the interaction between orbital and millennial-scale variability, which remains underexplored.

Our results suggest that central India was wetter and more forested during MIS 11 than during the pre-industrial period, reinforcing the importance of continued research on this interglacial to better understand the potential impacts of increased monsoon rainfall on tropical forest dynamics and biodiversity.

Data availability

The pollen record from Site U1446 presented in this manuscript is available online in the PANGAEA data repository (Oliveira et al., 2025).

Author contributions

D.O. conducted the pollen analyses, with contributions from S.D., S.P., K.A. and C.Z., and designed the research. Q.Y. and Z.W. performed the climate-model experiments. D.O. led the manuscript writing, with input from all authors. Funding acquisition by P.M., S.D. and D.O.

Competing interests

At least one of the (co-)authors is a member of the editorial board of Climate of the Past. The authors have no other competing interests to declare.

Acknowledgements

This research was funded by the Portuguese Foundation for Science and Technology (FCT) through projects INDRA (EXPL/CTA-CLI/0612/2021) and Hydroshifts (PTDC/CTA-CLI/4297/2021), CCMAR projects UIDB/04326/2020 (https://doi.org/10.54499/UIDB/04326/2020), UIDP/04326/2020 (https://doi.org/10.54499/UIDP/04326/2020), and CIMAR laboratory funding LA/P/0101/2020 (https://doi.org/10.54499/LA/P/0101/2020), and contracts for D. Oliveira (CEECIND/02208/2017) and C. Zorzi (CEECIND/CP1729/CT0001). Additional funding was provided from the French LEFE program (INSU-CNRS, project MICMAc) and IODP France. Computational resources were provided by Université Catholique de Louvain (CISM/UCL) and CÉCI, funded by F.R.S.-FNRS (convention 2.5020.11) and the Walloon Region. We thank the IODP Expedition 353 team, L. Devaux, M. Georget for technical support, and V. Hanquiez for Fig. 1.

References

Alonso-Garcia, M., Rodrigues, T., Abrantes, F., Padilha, M., Alvarez-Zarikian, C. A., Kunkelova, T., Wright, J. D., and Betzler, C.: Sea-surface temperature, productivity and hydrological changes in the Northern Indian Ocean (Maldives) during the interval ~575-175 ka (MIS 14 to 7), Palaeogeogr. Palaeoclimatol. Palaeoecol., 536, 109376, https://doi.org/10.1016/j.palaeo.2019.109376, 2019.

Anupama, K., Ramesh, B. R., and Bonnefille, R.: Modern pollen rain from the Biligirirangan–Melagiri hills of southern eastern Ghats, India, Rev. Palaeobot. Palynol., 108, 175–196, https://doi.org/10.1016/S0034-6667(99)00039-1, 2000.

Barboni, D.: Signal pollinique et climat de mousson en Inde du Sud, Aix-Marseille 3, 2000.

Barboni, D. and Bonnefille, R.: Precipitation signal in pollen rain from tropical forests, South India, Rev. Palaeobot. Palynol., 114, 239–258, https://doi.org/10.1016/S0034-6667(01)00057-4, 2001.

Barboni, D., Bonnefille, R., Prasad, S., and Ramesh, B.: Variation in modern pollen from tropical evergreen forests and the monsoon seasonality gradient in SW India, J. Veg. Sci., 14, 551–562, https://doi.org/10.1111/j.1654-1103.2003.tb02182.x, 2003.

Barker, S., Chen, J., Gong, X., Jonkers, L., Knorr, G., and Thornalley, D.: Icebergs not the trigger for North Atlantic cold events, Nature, 520, 333–336, https://doi.org/10.1038/nature14330, 2015.

Barker, S., Knorr, G., Conn, S., Lordsmith, S., Newman, D., and Thornalley, D.: Early interglacial legacy of deglacial climate instability, Paleoceanogr. Paleoclimatol., 34, 1455–1475, https://doi.org/10.1029/2019PA003661, 2019.

Barker, S., Knorr, G., Edwards, R. L., Parrenin, F., Putnam, A. E., Skinner, L. C., Wolff, E., and Ziegler, M.: 800,000 years of abrupt climate variability, Science, 334, 347–351, https://doi.org/10.1126/science.1203580, 2011.

Basumatary, S. K., Bera, S. K., Sangma, S. N., and Marak, G.: Modern pollen deposition in relation to vegetation and climate of Balpakram valley, Meghalaya, northeast India: Implications for Indo-Burma palaeoecological contexts, Quat. Int., 325, 30–40, https://doi.org/10.1016/j.quaint.2013.08.013, 2014.

Batchelor, C. J., McGee, D., Shakun, J. D., Woodhead, J., Jost, A. B., and Arnold, S.: Insights into changing interglacial conditions in subarctic Canada from MIS 11 through MIS 5e from seasonally resolved speleothem records, Geophys. Res. Lett., 51, e2024GL108459, https://doi.org/10.1029/2024GL108459, 2024.

Baumgartner, M., Schilt, A., Eicher, O., Schmitt, J., Schwander, J., Spahni, R., Fischer, H., and Stocker, T. F.: High-resolution interpolar difference of atmospheric methane around the Last Glacial Maximum, Biogeosciences, 9, 3961–3977, https://doi.org/10.5194/bg-9-3961-2012, 2012.

Bennett, K.: Psimpoll and Pscomb software, Queen's University Belfast, 2008.

Berger, A. and Loutre, M. F.: Insolation values for the climate of the last 10 million years, Quat. Sci. Rev., 10, 297–317, https://doi.org/10.1016/0277-3791(91)90033-Q, 1991.

Berger, A. and Loutre, M. F.: An exceptionally long interglacial ahead? Science, 297, 1287–1288, 2002.

Bhadra, S. R. and Saraswat, R.: A strong influence of the mid-Pleistocene transition on the monsoon and associated productivity in the Indian Ocean, Quat. Sci. Rev., 295, 107761, 2022.

Birks, H. and Birks, H.: Quaternary palaeoecology, Edward Arnold, 1980.

Bock, M., Schmitt, J., Beck, J., Seth, B., Chappellaz, J., and Fischer, H.: Glacial/interglacial wetland, biomass burning, and geologic methane emissions constrained by dual stable isotopic CH_4 ice core records, Proc. Natl. Acad. Sci. U.S.A., 114, E5778–E5786, https://doi.org/10.1073/pnas.1613883114, 2017.

Bolton, C. T., Clemens, S. C., Kodama, K., Ikehara, M., Medina-Elizalde, M., Paterson, G. A., and Chang, L.: A 500,000 year record of Indian summer monsoon dynamics recorded by eastern equatorial Indian Ocean upper water-column structure, Paleoceanogr., 28, 386–400, https://doi.org/10.1002/palo.20036, 2013.

Bond, W. J. and Midgley, G. F.: A proposed CO_2-controlled mechanism of woody plant invasion in grasslands and savannas, Global Change Biol., 6, 865–869, https://doi.org/10.1046/j.1365-2486.2000.00365.x, 2000.

Bonnefille, R., Anupama, K., Barboni, D., Pascal, J., Prasad, S., and Sutra, J. P.: Modern pollen spectra from tropical South India and Sri Lanka: Altitudinal distribution, J. Biogeogr., 26, 1255–1280, https://doi.org/10.1046/j.1365-2699.1999.00359, 1999.

Brandon, M., Landais, A., Duchamp-Alphonse, S., Favre, V., Schmitz, L., Abrial, H., Prie, F., Extier, T., and Blunier, T.: Exceptionally high biosphere productivity at the beginning of Marine Isotopic Stage 11, Nat. Commun., 11, 2112, https://doi.org/10.1038/s41467-020-15739-2, 2020.

Brönnimann, S.: Impact of El Niño–Southern Oscillation on European climate, Rev. Geophys., 45, RG3003, https://doi.org/10.1029/2006RG000199, 2007.

Brovkin, V., Ganapolski, A., and Svirezhev, Y.: A continuous climate vegetation classification for use in climate-biosphere studies, Ecol. Model., 101, 251–261, 1997.

Caley, T., Malaizé, B., Zaragosi, S., Rossignol, L., Bourget, J., Eynaud, F., Martinez, P., Giraudeau, J., Charlier, K., and Ellouz-Zimmermann, N.: New Arabian Sea records help decipher orbital timing of Indo-Asian monsoon, Earth Planet. Sci. Lett., 308, 433–444, https://doi.org/10.1016/j.epsl.2011.06.019, 2011.

Candy, I., McGee, D., Sherriff, J., Coxon, P., McClymont, E., and Schreve, D. C.: The climatic structure of MIS 11 in Britain, J. Quat. Sci., 31, 75–92, https://doi.org/10.1111/jqs.12076, 2014.

Candy, I., Oliveira, D., Parkes, D., Sherriff, J., and Thornalley, D.: Marine Isotope Stage 11c in Europe: Recent advances in marine–terrestrial correlations and their implications for interglacial stratigraphy – A review, Boreas, https://doi.org/10.1111/bor.12656, 2024.

Cerling, T. E., Ehleringer, J. R., and Harris, J. M.: Carbon dioxide starvation, the development of C4 ecosystems, and mammalian evolution, Philos. Trans. R. Soc. Lond., B Biol. Sci., 353, 159–171, https://doi.org/10.1098/rstb.1998.0207, 1998.

Champion, S. H. G., and Seth, S. K.: A revised survey of the forest types of India, 1968.

Cheng, H., Edwards, R. L., Sinha, A., Spötl, C., Yi, L., Chen, S., and Kelly, M.: The Asian monsoon over the past 640,000 years and ice age terminations, Nature, 534, 640–646, https://doi.org/10.1038/nature18591, 2016.

Cheng, H., Li, H., Sha, L., Sinha, A., Shi, Z., Yin, Q., Lu, Z., Zhao, D., Cai, Y., Hu, Y., Hao, Q., Tian, J., Kathayat, G., Dong, X., Zhao, J., and Zhang, H.: Milankovitch theory and monsoon, Innov., 3, 100338, https://doi.org/10.1016/j.xinn.2022.100338, 2022.

Chiang, J. C. H., and Bitz, C. M.: Influence of high latitude ice cover on the marine intertropical convergence zone, Clim. Dyn., 25, 477–496, https://doi.org/10.1007/s00382-005-0040-5, 2005.

Clemens, S. C., and Prell, W. L.: A 350,000-year summer-monsoon multi-proxy stack from the Owen Ridge, Northern Arabian Sea, Mar. Geol., 201, 35–51, https://doi.org/10.1016/S0025-3227(03)00207-X, 2003.

Clemens, S. C., Holbourn, A., Kubota, Y., Lee, K. E., Liu, Z., Chen, G., Nelson, A., and Fox-Kemper, B.: Precession-band variance missing from East Asian monsoon runoff, Nat. Commun., 9, https://doi.org/10.1038/s41467-018-05814-0, 2018.

Clemens, S. C., Yamamoto, M., Thirumalai, K., Giosan, L., Richey, J. N., Nilsson-Kerr, K., Rosenthal, Y., Anand, P., and McGrath, S. M.: Remote and local drivers of Pleistocene South Asian summer monsoon precipitation: A test for future predictions, Sci. Adv., 7, eabg3848, https://doi.org/10.1126/sciadv.abg3848, 2021.

Clément, C., Martinez, P., Yin, Q., Clemens, S., Thirumalai, K., Prasad, S., Anupama, K., Su, Q., Lyu, A., Grémare, A., and Desprat, S.: Greening of India and revival of the South Asian summer monsoon in a warmer world, Commun Earth Environ 5, 685, https://doi.org/10.1038/s43247-024-01781-1, 2024.

Cleveland, W. S., Grosse, E., and Shyu, W. M.: Local regression models, in: Statistical models in S, edited by: Chambers, J. M., and Hastie, T. J., Wadsworth and Brooks/Cole, 608, 1992.

de Vernal, A., and Hillaire-Marcel, C.: Natural variability of Greenland climate, vegetation, and ice volume during the past million years, Science, 320, 1622–1625, https://doi.org/10.1126/science.1153929, 2008.

Desprat, S., Oliveira, D., Naughton, F., and Sánchez Goñi, M. F.: L'étude du pollen des séquences sédimentaires marines pour la compréhension du climat: L'exemple des périodes chaudes passées, Quaternaire, 28, 259–269, https://doi.org/10.4000/quaternaire.7844, 2017.

Desprat, S., Sánchez Goñi, M. F., Turon, J. L., McManus, J. F., Loutre, M. F., Malaizé, B., and Peyron, O.: Is vegetation responsible for glacial inception during periods of muted insolation changes?, Quat. Sci. Rev., 24, 1361–1374, https://doi.org/10.1016/j.quascirev.2005.01.001, 2005.

Dong, B., Sutton, R.T.: Enhancement of ENSO variability by a weakened Atlantic thermohaline circulation in a coupled GCM. Journal of Climate, 20, 4920–4939. https://doi.org/10.1175/JCLI4284.1.

Droxler, A. W., Alley, R. B., Howard, W. R., Poore, R. Z., and Burckle, L. H.: Unique and exceptionally long interglacial Marine Isotope Stage 11: Window into Earth's warm future climate, in: Earth's Climate and Orbital Eccentricity: The Marine Isotope Stage 11 Question, edited by: Droxler, A. W., Poore, R. Z., and Burckle, L. H., Geophys. Monogr. Ser., Blackwell Publ., 1–14, 2003.

Dupont, L. M., and Agwu, C. O. C.: Latitudinal shifts of forest and savanna in NW Africa during the Brunhes chron: Further marine palynological results from site M16415 (9°N, 19°W), Veg. Hist. Archaeobot., 1, 163–175, https://doi.org/10.1007/BF00195279, 1992.

Dupont, L. M., Marret, F., and Winn, K.: Land-sea correlation by means of terrestrial and marine palynomorphs from the equatorial East Atlantic: Phasing of SE trade winds and oceanic productivity, Palaeogeogr. Palaeoclimatol. Palaeoecol., 142, 51–84, https://doi.org/10.1016/S0031-0182(98)00045-2, 1998.

Dutt, S., Gupta, A. K., Clemens, S. C., Cheng, H., Singh, R. K., Kathayat, G., and Edwards, R. L.: Abrupt changes in Indian summer monsoon strength during 33,800 to 5,500 years B.P., Geophys. Res. Lett., 42, 5526–5532, https://doi.org/10.1002/2015GL064015, 2015.

Dutton, A., Carlson, A. E., Long, A. J., Milne, G. A., Clark, P. U., DeConto, R., Horton, B. P., Rahmstorf, S., and Raymo, M. E.: Sea-level rise due to polar ice-sheet mass loss during past warm periods, Science, 349, aaa4019, https://doi.org/10.1126/science.aaa4019, 2015.

Ehleringer, J. R., Cerling, T. E., and Helliker, B. R.: C4 photosynthesis, atmospheric CO_2, and climate, Oecologia, 112, 285–299, https://doi.org/10.1007/s004420050311, 1997.

Fairchild, I. J., and Baker, A.: Speleothem Science: From Process to Past Environment, Wiley-Blackwell, Chichester, UK, 2012.

Fawcett, P. J., Werne, J. P., Anderson, R. S., Heikoop, J. M., Brown, E. T., Berke, M. A., Smith, S. J., Goff, F., Donohoo-Hurley, L., Cisneros-Dozal, L. M., Schouten, S., Sinninghe Damsté, J. S., Huang, Y., Toney, J., Fessenden, J., WoldeGabriel, G., Atudorei, V., Geissman, J. W., and Allen, C. D.: Extended megadroughts in the southwestern United States during Pleistocene interglacials, Nature, 470, 518–521, https://doi.org/10.1038/nature09839, 2011.

Gadgil, S.: The Indian monsoon and its variability, Annu. Rev. Earth Planet. Sci., 31, 429–467, https://doi.org/10.1146/annurev.earth.31.100901.141251, 2003.

Gadgil, S.: The monsoon system: Land–sea breeze or the ITCZ?, J. Earth Syst. Sci., 127, 1, https://doi.org/10.1007/s12040-017-0916-x, 2018.

Gadgil, S., Rajeevan, M., and Francis, P. A.: Monsoon variability: Links to major oscillations over the equatorial Pacific and Indian Oceans, Curr. Sci., 93, 182–194, 2007.

Galaasen, E.V., Ninnemann, U.S., Kessler, A., Irvalı, N., Rosenthal, Y., Tjiputra, J., Bouttes, N., Roche, D.M., Kleiven, H. (Kikki) F., Hodell, D.A., 2020. Interglacial instability of North Atlantic Deep Water ventilation. Science, 367, 1485–1489. https://doi.org/10.1126/science.aay6381.

Gao, X., Hao, Q., Wang, L., Song, Y., Ge, J., Wu, H., Xu, B., Han, L., Fu, Y., Wu, X., Deng, C., and Guo, Z.: Changes in monsoon precipitation in East Asia under a 2°C interglacial warming, Sci. Adv., 10, eadm7694, https://doi.org/10.1126/sciadv.adm7694, 2024.

Gebregiorgis, D., Hathorne, E. C., Giosan, L., Clemens, S., Nürnberg, D., and Frank, M.: Southern Hemisphere forcing of South Asian monsoon precipitation over the past ~1 million years, Nat. Commun., 9, 4702, https://doi.org/10.1038/s41467-018-07076-2, 2018.

Georget, M., Castéra, M.-H., Devaux, L., Turon, J.-L., Desprat, S., Sanchez Goni, M.F.: Protocol for pollen and dinocyst analysis in marine sediments, Protocols.io, https://doi.org/dx.doi.org/10.17504/protocols.io.x54v92qz4l3e/v1, 2025.

Gosling, W. D., Miller, C. S., and Livingstone, D. A.: Atlas of the tropical West African pollen flora, Rev. Palaeobot. Palynol., 199, 1–135, https://doi.org/10.1016/j.revpalbo.2013.01.003, 2013.

Goswami, B. B., and An, S.-I.: An assessment of the ENSO-monsoon teleconnection in a warming climate, npj Clim. Atmos. Sci., 6, 82, https://doi.org/10.1038/s41612-023-00411-5, 2023.

Goswami, B. N., and Chakravorty, S.: Dynamics of the Indian Summer Monsoon Climate, Oxford Univ. Press, 2017.

Gunnell, Y.: Relief and climate in South Asia: The influence of the western ghats on the current climate pattern of peninsular India, Int. J. Climatol., 17, 1169–1182, https://doi.org/10.1002/(SICI)1097-0088(199709)17:11<1169::AID-JOC189>3.0.CO;2-W, 1997.

Guo, Z., Zhou, X., and Wu, H.: Glacial-interglacial water cycle, global monsoon and atmospheric methane changes, Clim. Dyn., 39, 1073–1092, https://doi.org/10.1007/s00382-011-1147-5, 2012.

Harrison, S.P., Prentice, C.I.: Climate and CO2 controls on global vegetation distribution at the last glacial maximum: analysis based on palaeovegetation data, biome modelling and palaeoclimate simulations. Global Change Biology 9, 983–1004. https://doi.org/10.1046/j.1365-2486.2003.00640.x, 2003.

Hayashi, R., Sagawa, T., Irino, T., and Tada, R.: Orbital-scale vegetation-ocean-atmosphere linkages in western Japan during the last 550 ka based on a pollen record from the IODP site U1427 in the Japan Sea, Quat. Sci. Rev., 267, 107103, https://doi.org/10.1016/j.quascirev.2021.107103, 2021.

Hes, G., Sanchez Goñi, M. F., and Bouttes, N.: Impact of terrestrial biosphere on the atmospheric CO_2 concentration across Termination V, Clim. Past, 18, 1429–1451, 2022.

Hodell, D. A., Channell, J. E. T., Curtis, J. H., Romero, O. E., and Röhl, U.: Onset of "Hudson Strait" Heinrich events in the eastern North Atlantic at the end of the middle Pleistocene transition (~640 ka)?, Paleoceanography, 23, 1–16, https://doi.org/10.1029/2008PA001591, 2008.

Hodell, D. A., Crowhurst, S. J., Lourens, L., Margari, V., Nicolson, J., Rolfe, J. E., Skinner, L. C., Thomas, N. C., Tzedakis, P. C., Mleneck-Vautravers, M. J., and Wolff, E. W.: A 1.5-million-year record of orbital and millennial climate variability in the North Atlantic, Clim. Past, 19, 327–350, https://doi.org/10.5194/cp-19-327-2023, 2023.

Goosse, H., Brovkin, V., Fichefet, T., Haarsma, R., Huybrechts, P., Jongma, J., Mouchet, A., Selten, F., Barriat, P.-Y., Campin, J.-M., Deleersnijder, E., Driesschaert, E., Goelzer, H., Janssens, I., Loutre, M.-F., Maqueda, M. A., Opsteegh, T., Mathieu, P.-P., Munhoven, G., Pettersson, E. J., Renssen, H., Roche, D. M., Schaeffer, M., Tartinville, B., Timmermann, A., and Weber, S. L.: Description of the Earth system model of intermediate complexity LOVECLIM version 1.2, Geosci. Model Dev., 3, 603–633, https://doi.org/10.5194/gmd-3-603-2010, 2010.

Hrudya, P. H., Varikoden, H., and Vishnu, R.: A review on the Indian summer monsoon rainfall, variability and its association with ENSO and IOD, Meteorol. Atmos. Phys., 11, 421, https://doi.org/10.1007/s00703-020-00734-5, 2020.

Hu, H.-M., Marino, G., Pérez-Mejías, C., Spötl, C., Yokoyama, Y., Yu, J., Rohling, E., Kano, A., Ludwig, P., Pinto, J. G., Michel, V., Valensi, P., Zhang, X., Jiang, X., Mii, H.-S., Chien, W.-Y., Tsai, H.-C., Sung, W.-H., Hsu, C.-H., Starnini, E., Zunino, M., and Shen, C.-C.: Sustained North Atlantic warming drove anomalously intense MIS 11c interglacial, Nat. Commun., 15, 5933, https://doi.org/10.1038/s41467-024-50207-1, 2024.

Hu, J., Emile-Geay, J., Tabor, C., Nusbaumer, J., and Partin, J.: Deciphering oxygen isotope records from Chinese speleothems with an isotope-enabled climate model, Paleoceanogr. Paleoclimatol., 34, 2098–2112, https://doi.org/10.1029/2019PA003741, 2019.

IPCC: Climate Change 2022: Impacts, Adaptation, and Vulnerability. Contribution of Working Group II to the Sixth Assessment Report of the Intergovernmental Panel on Climate Change, edited by: Pörtner, H.-O., Roberts, D. C., Tignor, M., Poloczanska, E. S., Mintenbeck, K., Alegría, A., Craig, M., Langsdorf, S., Löschke, S., Möller, V., Okem, A., and Rama, B., Cambridge Univ. Press, 3056 pp., https://doi.org/10.1017/9781009325844, 2022.

Jalihal, C., Bosmans, J. H. C., Srinivasan, J., and Chakraborty, A.: The response of tropical precipitation to Earth's precession: The role of energy fluxes and vertical stability, Clim. Past, 15, 449–462, https://doi.org/10.5194/cp-15-449-2019, 2019.

Jouzel, J., Masson-Delmotte, V., Cattani, O., Dreyfus, G., Falourd, S., Hoffmann, G., Minster, B., Nouet, J., Barnola, J. M., Chappellaz, J., Fischer, H., Gallet, J. C., Johnsen, S., Leuenberger, M., Loulergue, L., Luethi, D., Oerter, H., Parrenin, F., Raisbeck, G., Raynaud, D., Schilt, A., Schwander, J., Selmo, E., Souchez, R., Spahni, R., Stauffer, B., Steffensen, J. P., Stenni, B., Stocker, T. F., Tison, J. L., Werner, M., and Wolff, E. W.: Orbital and millennial Antarctic climate variability over the past 800,000 years, Science, 317, 793–796, https://doi.org/10.1126/science.1141038, 2007.

Juggins, S.: Package "rioja" – Analysis of Quaternary Science Data, CRAN, 2009.

Kageyama, M., Harrison, S.P., Kapsch, M.-L., Lofverstrom, M., Lora, J.M., Mikolajewicz, U., Sherriff-Tadano, S., Vadsaria, T., Abe-Ouchi, A., Bouttes, N., Chandan, D., Gregoire, L.J., Ivanovic, R.F., Izumi, K., LeGrande, A.N., Lhardy, F., Lohmann, G., Morozova, P.A., Ohgaito, R., Paul, A., Peltier, W.R., Poulsen, C.J., Quiquet, A., Roche, D.M., Shi, X., Tierney, J.E., Valdes, P.J., Volodin, E., Zhu, J.: The PMIP4 Last Glacial Maximum experiments: preliminary results and comparison with the PMIP3 simulations. Clim. Past 17, 1065–1089. https://doi.org/10.5194/cp-17-1065-2021, 2021.

Kandiano, E. S., van der Meer, M. T. J., Schouten, S., Fahl, K., Sinninghe Damsté, J. S., and Bauch, H. A.: Response of the North Atlantic surface and intermediate ocean structure to climate warming of MIS 11, Sci. Rep., 7, 46192, https://doi.org/10.1038/srep46192, 2017.

Kathayat, G., Cheng, H., Sinha, A., Spötl, C., Edwards, R. L., Zhang, H., Li, X., Yi, L., Ning, Y., Cai, Y., Liu, W. L., and Breitenbach, S. F. M.: Indian monsoon variability on millennial-orbital timescales, Sci. Rep., 6, https://doi.org/10.1038/srep24374, 2016.

Katzenberger, A., Levermann, A., Schewe, J., and Pongratz, J.: Intensification of very wet monsoon seasons in India under global warming, Geophys. Res. Lett., 49, e2022GL098856, https://doi.org/10.1029/2022GL098856, 2022.

Katzenberger, A., Schewe, J., Pongratz, J., and Levermann, A.: Robust increase of Indian monsoon rainfall and its variability under future warming in CMIP6 models, Earth Syst. Dyn., 12, 367–386, 2021.

Kirschke, S., Bousquet, P., Ciais, P., Saunois, M., Canadell, J. G., Dlugokencky, E. J., Bergamaschi, P., Bergmann, D., Blake, D. R., Bruhwiler, L., Cameron-Smith, P., Castaldi, S., Chevallier, F., Feng, L., Fraser, A., Heimann, M., Hodson, E. L., Houweling, S., Josse, B., Fraser, P. J., Krummel, P. B., Lamarque, J.-F., Langenfelds, R. L., LeQuéré, C., Naik, V., O'Doherty, S., Palmer, P. I., Pison, I., Plummer, D., Poulter, B., Prinn, R. G., Rigby, M., Ringeval, B., Santini, M., Schmidt, M., Shindell, D. T., Simpson, I. J., Spahni, R., et al.: Three decades of global methane sources and sinks, Nat. Geosci., https://doi.org/10.1038/ngeo1955, 2013.

Kleinen, T., Hildebrandt, S., Prange, M., Rachmayani, R., Müller, S., Bezrukova, E., Brovkin, V., and Tarasov, P. E.: The climate and vegetation of Marine Isotope Stage 11: Model results and proxy-based reconstructions at global and regional scale, Quat. Int., 348, 247–265, https://doi.org/10.1016/j.quaint.2013.12.028, 2014.

Kottek, M., Grieser, J., Beck, C., Rudolf, B., Rubel, F.: World Map of the Köppen-Geiger climate classification updated. metz 15, 259–263. https://doi.org/10.1127/0941-2948/2006/0130, 2006.

Kousis, I., Koutsodendris, A., Peyron, O., Leicher, N., Francke, A., Wagner, B., Giaccio, B., Knipping, M., and Pross, J.: Centennial-scale vegetation dynamics and climate variability in SE Europe during Marine Isotope Stage 11 based on a pollen record from Lake Ohrid, Quat. Sci. Rev., 190, 20–38, https://doi.org/10.1016/j.quascirev.2018.04.027, 2018.

Krishnamurthy, V., and Goswami, B. N.: Indian Monsoon–ENSO relationship on interdecadal timescale, J. Clim., 13, 579–595, 2000.

Kumar, K. K., Rajagopalan, B., and Cane, M. A.: On the weakening relationship between the Indian monsoon and ENSO, Science, 284, 2156–2159, 1999.

Kutzbach, J. E., Liu, X. D., Liu, Z. Y., and Chen, G. S.: Simulation of the evolutionary response of global summer monsoons to orbital forcing over the past 280,000 years, Clim. Dyn., 30, 567–579, https://doi.org/10.1007/s00382-007-0308-z, 2008.

Kutzbach, J. E.: Monsoon climate of the early Holocene: climate experiment with the Earth's orbital parameters for 9000 years ago, Science, 214, 59–61, 1981.

Legris, P.: La végétation de l’Inde, écologie et flore, Trav. Sect. Sci. Tech., Inst. Fr. Pondichery, 6, 622, 1963.

Lisiecki, L. E., and Raymo, M. E.: A Pliocene-Pleistocene stack of 57 globally distributed benthic δ18O records, Paleoceanography, 20, PA1003, https://doi.org/10.1029/2004PA001071, 2005.

Liu, Y., Wu, Y., Lin, Z., Zhang, Y., Zhu, J., Yi, C.: Simulated Impact of the Tibetan Glacier Expansion on the Eurasian Climate and Glacial Surface Mass Balance during the Last Glacial Maximum. Journal of Climate 33, 6491–6509. https://doi.org/10.1175/JCLI-D-19-0763.1, 2020a.

Liu, G., Li, X., Chiang, H.-W., Cheng, H., Yuan, S., Chawchai, S., He, S., Lu, Y., Aung, L.T., Maung, P.M., Tun, W.N., Oo, K.M., Wang, X.: On the glacial-interglacial variability of the Asian monsoon in speleothem $\delta^{18}O$ records. Sci Adv 6, eaay8189. https://doi.org/10.1126/sciadv.aay8189, 2020b.

Liu, W., Wang, G., Yu, M., Chen, H., Jiang, Y., Yang, M., and Shi, Y.: Projecting the future vegetation–climate system over East Asia and its RCP-dependence, Clim. Dyn., 55, 2725–2742, https://doi.org/10.1007/s00382-020-05411-2, 2020c.

Lyu, A. Q., Yin, Q. Z., Crucifix, M., and Sun, Y. B.: Diverse regional sensitivity of summer precipitation in East Asia to ice volume, CO_2, and astronomical forcing, Geophys. Res. Lett., 48, https://doi.org/10.1029/2020GL092005, 2021.

Marzin, C., Kallel, N., Kageyama, M., Duplessy, J.-C., and Braconnot, P.: Glacial fluctuations of the Indian monsoon and their relationship with North Atlantic climate: New data and modelling experiments, Clim. Past, 9, 2135–2151, https://doi.org/10.5194/cp-9-2135-2013, 2013.

McAndrews, J. H., and King, J. E.: Pollen of the North American Quaternary: The top twenty, Geosci. Man, 15, 41–49, 1976.

McGee, D., Donohoe, A., Marshall, J., and Ferreira, D.: Changes in ITCZ location and cross-equatorial heat transport at the last glacial maximum, Heinrich stadial 1, and the mid-Holocene, Earth Planet. Sci. Lett., 390, 69–79, https://doi.org/10.1016/j.epsl.2013.12.043, 2014.

McGrath, S. M., Clemens, S. C., Huang, Y., and Yamamoto, M.: Greenhouse gas and ice volume drive Pleistocene Indian summer monsoon precipitation isotope variability, Geophys. Res. Lett., 48, e2020GL092249, https://doi.org/10.1029/2020GL092249, 2021.

McManus, J. F., Oppo, D. W., and Cullen, J. L.: A 0.5-million-year record of millennial-scale climate variability in the North Atlantic, Science, 283, 971–974, https://doi.org/10.1126/science.283.5404.971, 1999.

Mehrotra, N., Shah, S. K., Basavaiah, N., and Kar, R.: Middle to Late Holocene climate, vegetation and sea-level changes in NW Tripura, northeast India, based on palynological and mineral magnetic evidence, J. Paleolimnol., 68, 297–313, https://doi.org/10.1007/s10933-022-00249-6, 2022.

Melles, M., Brigham-Grette, J., Minyuk, P. S., Nowaczyk, N. R., Wennrich, V., DeConto, R. M., Anderson, P. M., Andreev, A. A., Coletti, A., Cook, T. L., and Wagner, B.: 2.8 million years of Arctic climate change from Lake El'gygytgyn, NE Russia, Science, 337, 315–320, https://doi.org/10.1126/science.1222135, 2012.

Mohtadi, M., Prange, M., and Steinke, S.: Palaeoclimatic insights into forcing and response of monsoon rainfall, Nature, 533, 191–199, https://doi.org/10.1038/nature17450, 2016.

Mohtadi, M., Prange, M., Oppo, D. W., De Pol-Holz, R., Merkel, U., Zhang, X., Steinke, S., and Lückge, A.: North Atlantic forcing of tropical Indian Ocean climate, Nature, 509, 76–80, https://doi.org/10.1038/nature13196, 2014.

Nehrbass-Ahles, C., Shin, J., Schmitt, J., Bereiter, B., Joos, F., Schilt, A., Schmidely, L., Silva, L., Teste, G., Grilli, R., Chappellaz, J., Hodell, D., Fischer, H., and Stocker, T. F.: Abrupt CO_2 release to the atmosphere under glacial and early interglacial climate conditions, Science, 369, 1000–1005, https://doi.org/10.1126/science.aay8178, 2020.

Nilsson-Kerr, K., Anand, P., Holden, P. B., Clemens, S. C., and Leng, M. J.: Dipole patterns in tropical precipitation were pervasive across landmasses throughout Marine Isotope Stage 5, Commun. Earth Environ., 2, 64, https://doi.org/10.1038/s43247-021-00133-7, 2021.

Nilsson-Kerr, K., Anand, P., Sexton, P. F., Leng, M. J., Misra, S., Clemens, S. C., and Hammond, S. J.: Role of Asian summer monsoon subsystems in the inter-hemispheric progression of deglaciation, Nat. Geosci., 12, 290–295, https://doi.org/10.1038/s41561-019-0327-1, 2019.

Oliveira, D., Desprat, S., Rodrigues, T., Naughton, F., Hodell, D., Trigo, R., Rufino, M., Lopes, C., Abrantes, F., and Sánchez Goñi, M. F.: The complexity of millennial-scale variability in southwestern Europe during MIS 11, Quat. Res., 86, 373–387, https://doi.org/10.1016/j.yqres.2016.09.002, 2016.

Oliveira, D., Desprat, S., Yin, Q., Naughton, F., Trigo, R., Rodrigues, T., Abrantes, F., and Sánchez Goñi, M. F.: Unraveling the forcings controlling the vegetation and climate of the best orbital analogues for the present interglacial in SW Europe, Clim. Dyn., 51, 667–684, https://doi.org/10.1007/s00382-017-3948-7, 2018.

Oliveira, D., Desprat, S., Yin, Q., Zorzi, C., Wu, Z., Anupama, K., Prasad, S., Alonso-Garcia, M., and Martinez, P.: Pollen-based vegetation record from IODP Site 353-U1446 (Bay of Bengal), Marine Isotope Stage 11, PANGAEA, https://doi.org/10.1594/PANGAEA.982497, 2025.

Oppo, D. W., McManus, J. F., and Cullen, J. L.: Abrupt climate events 500,000 to 340,000 years ago: Evidence from subpolar North Atlantic sediments, Science, 279, 1335–1338, 1998.

Ota, Y., Kawahata, H., Kuroda, J., Suzuki, A., Abe-Ouchi, A., Jimenez-Espejo, F. J., and JAMSTEC NGHP-02 Scientist Team: Millennial-scale variability of Indian summer monsoon constrained by the western Bay of Bengal sediments: Implications from geochemical proxies of sea surface salinity and river runoff, Glob. Planet. Change, 208, 103719, https://doi.org/10.1016/j.gloplacha.2021.103719, 2022.

Pan, C., Zhu, B., Gao, J., and Kang, H.: Source apportionment of atmospheric water over East Asia—a source tracer study in CAM5.1, Geosci. Model Dev., 10, 673–688, 2017.

Past Interglacials Working Group of PAGES: Interglacials of the last 800,000 years, Rev. Geophys., 54, 162–219, 2016.

Pausata, F.S.R., Chafik, L., Caballero, R., Battisti, D.S.: Impacts of high-latitude volcanic eruptions on ENSO and AMOC. PNAS, 112, 13784–13788, 2015.

Prell, W. L., and Kutzbach, J. E.: Sensitivity of the Indian monsoon to forcing parameters and implications for its evolution, Nature, 360, 647–652, https://doi.org/10.1038/360647a0, 1992.

Prokopenko, A. A., Bezrukova, E. V., Khursevich, G. K., Solotchina, E. P., Kuzmin, M. I., and Tarasov, P. E.: Climate in continental interior Asia during the longest interglacial of the past 500,000 years: The new MIS 11 records from Lake Baikal, SE Siberia, Clim. Past, 6, 31–48, https://doi.org/10.5194/cp-6-31-2010, 2010.

Prokopenko, A. A., Williams, D. F., Kuzmin, M. I., Karabanov, E. B., Khursevich, G. K., and Peck, J. A.: Muted climate variations in continental Siberia during the mid-Pleistocene epoch, Nature, 418, 65–68, https://doi.org/10.1038/nature00886, 2002.

Quamar, M. F., and Bera, S. K.: Modern pollen–vegetation relationship in the tropical mixed deciduous forest of the Koriya District in Chhattisgarh, India, Grana, 54, 45–52, https://doi.org/10.1080/00173134.2014.946443, 2015.

Raymo, M.E., Oppo, D.W., Flower, B.P., Hodell, D.A., McManus, J.F., Venz, K.A., Kleiven, K.F., McIntyre, K.: Stability of North Atlantic water masses in face of pronounced climate variability during the Pleistocene. Paleoceanography 19, PA2008 1-13, 2004.

R Core Team: R: A language and environment for statistical computing, R Found. Stat. Comput., 2014.

Rodrigues, T., Voelker, A. H. L., Grimalt, J. O., Abrantes, F., and Naughton, F.: Iberian Margin sea surface temperature during MIS 15 to 9 (580–300 ka): Glacial suborbital variability versus interglacial stability, Paleoceanography, 26, https://doi.org/10.1029/2010PA001927, 2011.

Sachse, D., Billault, I., Bowen, G. J., Chikaraishi, Y., Dawson, T. E., Feakins, S. J., et al.: Molecular paleohydrology: Interpreting the hydrogen-isotopic composition of lipid biomarkers from photosynthesizing organisms, Annu. Rev. Earth Planet. Sci., 40, 221–249, https://doi.org/10.1146/annurev-earth-042711-105535, 2012.

Sassoon, D., Lebreton, V., Combourieu-Nebout, N., Peyron, O., and Moncel, M. H.: Palaeoenvironmental changes in the southwestern Mediterranean (ODP Site 976, Alboran Sea) during the MIS 12/11 transition and the MIS 11 interglacial and implications for hominin populations, Quat. Sci. Rev., 304, 108010, https://doi.org/10.1016/j.quascirev.2023.108010, 2023.

Schneider, T., Bischoff, T., and Haug, G. H.: Migrations and dynamics of the Intertropical Convergence Zone, Nature, 513, 45–53, 2014.

Sharmila, S., Joseph, S., Sahai, A. K., Abhilash, S., and Chattopadhyay, R.: Future projection of Indian summer monsoon variability under climate change scenario: An assessment from CMIP5 climate models, Glob. Planet. Change, 124, 62–78, 2015.

Singarayer, J. S., Valdes, P. J., Friedlingstein, P., Nelson, S. R., and Beerling, D. J.: Late Holocene methane rise caused by orbitally controlled increase in tropical sources, Nature, 470, 82–85, https://doi.org/10.1038/nature09739, 2011.

Snyder, C. W.: Evolution of global temperature over the past two million years, Nature, 538, 226–228, https://doi.org/10.1038/nature19798, 2016.

Stein, R., Hefter, J., Grützner, J., Voelker, A., and Naafs, B. D. A.: Variability of surface water characteristics and Heinrich-like events in the Pleistocene midlatitude North Atlantic Ocean: Biomarker and XRD records from IODP Site U1313 (MIS 16–9), Paleoceanography, 24, PA2203, https://doi.org/10.1029/2008PA001639, 2009.

Su, Q. Q., Lyu, A. Q., Wu, Z. P., and Yin, Q. Z.: Diverse response of global terrestrial vegetation to astronomical forcing and CO_2 during the MIS 11 and MIS 13 interglacials, Clim. Dyn., https://doi.org/10.1007/s00382-022-06308-y, 2022.

Sun, Y., Wang, T., Yin, Q., Lyu, A., Crucifix, M., Cai, Y., Ai, L., Clemens, S., and An, Z.: A review of orbital-scale monsoon variability and dynamics in East Asia during the Quaternary, Quat. Sci. Rev., 107593, https://doi.org/10.1016/j.quascirev.2022.107593, 2022.

Sun, Y., Yin, Q., Crucifix, M., Clemens, S. C., Araya-Melo, P., Liu, W., Qiang, X., Liu, Q., Zhao, H., Liang, L., Chen, H., Li, Y., Zhang, L., Dong, G., Li, M., Zhou, W., Berger, A., and An, Z.: Diverse manifestations of the mid-Pleistocene climate transition, Nat. Commun., 10, 352, https://doi.org/10.1038/s41467-018-08257-9, 2019.

Thanikaimoni, G.: Mangrove palynology, Travaux Sect. Sci. Tech., UNDP/UNESCO Regional Project on Training and Research on Mangrove Ecosystems, RAS/79/002, 1987.

Timmermann, A., Okumura, Y., An, S.-I., Clement, A., Dong, B., Guilyardi, E., Hu, A., Jungclaus, J.H., Renold, M., Stocker, T.F., Stouffer, R.J., Sutton, R., Xie, S.-P., Yin, J.: The Influence of a Weakening of the Atlantic Meridional Overturning Circulation on ENSO. Journal of Climate 20, 4899–4919. https://doi.org/10.1175/JCLI4283.1, 2007.

Tissot, C., Chikhi, H., and Nayar, T. S.: Pollen of wet evergreen forests of the Western Ghats, India, Publ. Dép. Écol., no. 35, Inst. Français de Pondichéry, Trav. Sect. Sci. Tech., 1994.

Torres, V., Hooghiemstra, H., Lourens, L., and Tzedakis, P. C.: Astronomical tuning of long pollen records reveals the dynamic history of montane biomes and lake levels in the tropical high Andes during the Quaternary, Quat. Sci. Rev., 63, 59–72, https://doi.org/10.1016/j.quascirev.2012.11.004, 2013.

Turner, A. G., and Slingo, J. M.: Uncertainties in future projections of extreme precipitation in the Indian monsoon region, Atmos. Sci. Lett., 10, 152–158, https://doi.org/10.1002/asl.223, 2009.

Tzedakis, P. C., Hodell, D. A., Nehrbass-Ahles, C., Mitsui, T., and Wolff, E. W.: Marine Isotope Stage 11c: An unusual interglacial, Quat. Sci. Rev., 284, 107493, https://doi.org/10.1016/j.quascirev.2022.107493, 2022.

Tzedakis, P. C., Pälike, H., Roucoux, K. H., and de Abreu, L.: Atmospheric methane, southern European vegetation and low-mid latitude links on orbital and millennial timescales, Earth Planet. Sci. Lett., 277, 307–317, https://doi.org/10.1016/j.epsl.2009.07.019, 2009.

Vaks, A., Gutareva, O. S., Breitenbach, S. F. M., Avirmed, E., Mason, A. J., Thomas, A. L., et al.: Speleothems reveal 500,000-year history of Siberian permafrost, Science, 340, 183–186, https://doi.org/10.1126/science.1228729, 2013.

Vaks, A., Mason, A. J., Breitenbach, S. F. M., Kononov, A. M., Osinzev, A. V., Rosensaft, M., et al.: Palaeoclimate evidence of vulnerable permafrost during times of low sea ice, Nature, 577, 221–225, https://doi.org/10.1038/s41586-019-1880-1, 2020.

Varghese, S. J., Surendran, S., Rajendran, K., and Kitoh, A.: Future projections of Indian Summer Monsoon under multiple RCPs using high-resolution global climate model multiforcing ensemble simulations, Clim. Dyn., 54, 1315–1328, 2020.

Wang, B., Liu, J., Kim, H.-J., Webster, P. J., Yim, S.-Y., and Xiang, B.: Northern Hemisphere summer monsoon intensified by mega-El Niño/Southern Oscillation and Atlantic multidecadal oscillation, Proc. Natl. Acad. Sci. USA, 110, 5347–5352, https://doi.org/10.1073/pnas.1219405110, 2013.

Wang, Y. V., Larsen, T., Lauterbach, S., Andersen, N., Blanz, T., Krebs-Kanzow, U., Gierz, P., and Schneider, R. R.: Higher sea surface temperature in the Indian Ocean during the Last Interglacial weakened the South Asian monsoon, Proc. Natl. Acad. Sci. USA, 119, e2107720119, https://doi.org/10.1073/pnas.2107720119, 2022.

Wang, Y., Yang, X., Wang, Y., Wang, Q., and Edwards, R. L.: The structure of marine isotope Stage 11 and its alignment with the Holocene, Palaeogeogr. Palaeoclimatol. Palaeoecol., 609, 111311, https://doi.org/10.1016/j.palaeo.2022.111311, 2023.

Webster, P. J., Magana, V. O., Palmer, T. N., Shukla, J., Tomas, R. A., Yanai, M., and Yasunari, T.: Monsoons: Processes, predictability, and the prospects for prediction, J. Geophys. Res., 103, 14451–14510, https://doi.org/10.1029/97JC02719, 1998.

Xiao, X. Y., Shen, J., Wang, S. M., Xiao, H. F., and Tong, G. B.: The variation of the southwest monsoon from the high-resolution pollen record in Heqing Basin, Yunnan Province, China, for the last 2.78 Ma, Palaeogeogr. Palaeoclimatol. Palaeoecol., 287, 45–57, https://doi.org/10.1016/j.palaeo.2010.01.013, 2010.

Yamamoto, M., Clemens, S. C., Seki, O., Tsuchiya, Y., Huang, Y., O'ishi, R., and Abe-Ouchi, A.: Increased interglacial atmospheric CO_2 levels followed the mid-Pleistocene Transition, Nat. Geosci., 15, 307–313, https://doi.org/10.1038/s41561-022-00918-1, 2022.

Yin, Q. Z., and Berger, A.: Individual contribution of insolation and CO_2 to the interglacial climates of the past 800,000 years, Clim. Dyn., 38, 709–724, https://doi.org/10.1007/s00382-011-1013-5, 2012.

Yin, Q., and Berger, A.: Interglacial analogues of the Holocene and its natural near future, Quat. Sci. Rev., 120, 28–46, https://doi.org/10.1016/j.quascirev.2015.04.008, 2015.

Yin, Q., Wu, Z. P., Berger, A., Goosse, H., and Hodell, D.: Insolation triggered abrupt weakening of Atlantic circulation at the end of interglacials, Science, 373, 1035–1040, https://doi.org/10.1126/science.abg1737, 2021.

Zhang, B., Li, Z., Kathayat, G., Tian, D., Baker, A., Wang, Z., Ning, E., Edwards, R. L., and Cheng, H.: The Asian Summer Monsoon: Teleconnections and Forcing Mechanisms—A Review from Chinese Speleothem δ18O Records, Quat., 2, 26, https://doi.org/10.3390/quat2030026, 2019.

Zhang, R., and Wang, B.: Global monsoon: A dominant mode of annual variations in the tropics, J. Clim., 21, 5033–5050, https://doi.org/10.1175/2008JCLI2053.1, 2008.

Zhang, Z., Liu, Z., Li, G., Cai, Y., Wen, Q., Cheng, H., Lawrence Edwards, R., Lei, J., Liu, H., Jing, Z., Li, T., Clemens, S.C., Wang, Y., Sun, Y., Shi, Z., Tan, L., Kang, S., Wang, X., Jin, Z., Zhou, W., An, Z.: Summer and nonsummer climatic signals in speleothem δ18O revealed by loess microcodium δ^{18}O in East Asia. Proceedings of the National Academy of Sciences 122, e2425565122. https://doi.org/10.1073/pnas.2425565122, 2025.

Zhao, X., Cheng, H., Sinha, A., Zhang, H., Baker, J. L., Chen, S., et al.: A high-resolution speleothem record of Marine Isotope Stage 11 as a natural analog to Holocene Asian summer monsoon variations, Geophys. Res. Lett., 46, 9949–9957, https://doi.org/10.1029/2019GL083836, 2019.

Zhao, Y., Tzedakis, P. C., Li, Q., Qin, F., Cui, Q., Liang, C., Birks, H. J. B., Liu, Y., Zhang, Z., Ge, J., Zhao, H., Felde, V. A., Deng, C., Cai, M., Li, H., Ren, W., Wei, H., Yang, H., Zhang, J., Yu, Z., and Guo, Z.: Evolution of vegetation and climate variability on the Tibetan Plateau over the past 1.74 million years, Sci. Adv., 6, eaay6193, https://doi.org/10.1126/sciadv.aay6193, 2020.

Zhisheng, A., Clemens, S. C., Shen, J., Qiang, X., Jin, Z., Sun, Y., Prell, W. L., Luo, J., Wang, S., Xu, H., Cai, Y., Zhou, W., Liu, X., Liu, W., Shi, Z., Yan, L., Xiao, X., Chang, H., Wu, F., Ai, L., and Lu, F.: Glacial-interglacial Indian summer monsoon dynamics, Science, 333, 719–723, https://doi.org/10.1126/science.1203752, 2011.

Ziegler, M., Lourens, L. J., Tuenter, E., Hilgen, F., Reichart, G.-J., and Weber, N.: Precession phasing offset between Indian summer monsoon and Arabian Sea productivity linked to changes in Atlantic overturning circulation, Paleoceanography, 25, https://doi.org/10.1029/2009PA001884, 2010.

Zorzi, C., Desprat, S., Clément, C., Thirumalai, K., Oliveira, D., Anupama, K., Prasad, S., and Martinez, P.: When Eastern India oscillated between desert versus savannah-dominated vegetation, Geophys. Res. Lett., 49, e2022GL099417, https://doi.org/10.1029/2022GL099417, 2022.

Zorzi, C., Sanchez Goñi, M. F., Anupama, K., Prasad, S., Hanquiez, V., Johnson, J., and Giosan, L.: Indian monsoon variations during three contrasting climatic periods: The Holocene, Heinrich Stadial 2 and the last interglacial–glacial transition, Quat. Sci. Rev., 125, 50–60, https://doi.org/10.1016/j.quascirev.2015.06.009, 2015.